



# Hygroscopic properties and cloud condensation nuclei activation of limonene-derived organosulfates and their mixtures with ammonium sulfate

A. M. K. Hansen<sup>1</sup>, J. Hong<sup>2</sup>, T. Raatikainen<sup>3</sup>, K. Kristensen<sup>1</sup>, A. Ylisirniö<sup>4</sup>, A. Virtanen<sup>4</sup>, T. Petäjä<sup>2</sup>, M. Glasius<sup>1</sup>, and N. L. Prisle<sup>2</sup>

<sup>1</sup>Department of Chemistry and iNANO, Aarhus University, Aarhus, Denmark

<sup>2</sup>Department of Physics, University of Helsinki, Helsinki, Finland

<sup>3</sup>Finnish Meteorological Institute, Helsinki, Finland

<sup>4</sup>Department of Applied Physics, University of Eastern Finland, Kuopio, Finland

Correspondence to: N. L. Prisle (nonne.prisle@helsinki.fi)

Received: 13 May 2015 – Published in Atmos. Chem. Phys. Discuss.: 25 June 2015

Revised: 18 November 2015 – Accepted: 4 December 2015 – Published: 21 December 2015

**Abstract.** Organosulfates have been observed as constituents of atmospheric aerosols in a wide range of environments; however their hygroscopic properties remain uncharacterised. Here, limonene-derived organosulfates with a molecular weight of 250 Da (L-OS 250) were synthesised and used for simultaneous measurements with a hygroscopicity tandem differential mobility analyser (H-TDMA) and a cloud condensation nuclei counter (CCNC) to determine the hygroscopicity parameter,  $\kappa$ , for pure L-OS 250 and mixtures of L-OS 250 with ammonium sulfate (AS) over a wide range of humidity conditions. The  $\kappa$  values derived from measurements with H-TDMA decreased with increasing particle dry diameter for all chemical compositions investigated, indicating that  $\kappa_{\text{H-TDMA}}$  depends on particle diameter and/or surface effects; however, it is not clear if this trend is statistically significant. For pure L-OS 250,  $\kappa$  was found to increase with increasing relative humidity, indicating dilution/solubility effects to be significant. Discrepancies in  $\kappa$  between the sub- and supersaturated measurements were observed for L-OS 250, whereas  $\kappa$  of AS and mixed L-OS 250/AS were similar. This discrepancy was primarily ascribed to limited dissolution of L-OS 250 at subsaturated conditions. In general, hygroscopic growth factor, critical particle diameter and  $\kappa$  for the mixed L-OS 250/AS particles converged towards the values of pure AS for mixtures with  $\geq 20\%$  w / w AS. Surface tension measurements of bulk aqueous L-OS 250/AS solutions showed that L-OS 250 was indeed surface active, as expected from its molecular structure, decreasing the sur-

face tension of solutions with 24 % from the pure water value at a L-OS 250 concentration of  $0.0025 \text{ mol L}^{-1}$ . Based on these surface tension measurements, we present the first concentration-dependent parametrisation of surface tension for aqueous L-OS 250, which was implemented to different process-level models of L-OS 250 hygroscopicity and CCN activation. The values of  $\kappa$  obtained from the measurements were compared with  $\kappa$  calculated applying the volume additive Zdanovskii–Stokes–Robinson mixing rule, as well as  $\kappa$  modelled from equilibrium Köhler theory with different assumptions regarding L-OS 250 bulk-to-surface partitioning and aqueous droplet surface tension. This study is to our knowledge the first to investigate the hygroscopic properties and surface activity of L-OS 250; hence it is an important first step towards understanding the atmospheric impact of organosulfates.

## 1 Introduction

Atmospheric aerosols still account for major uncertainties in our understanding of global climate and predictions of future climate changes (IPCC, 2013). Especially the indirect radiative effects of organic aerosols, i.e. their influence on cloud droplet formation and cloud properties, remain insufficiently constrained for reliable model predictions of both thermodynamic and large-scale general circulation levels (Hallquist

et al., 2009). Part of the uncertainty relates to our incomplete understanding of the various effects of mixing interactions in the aerosol phase – perhaps in particular the effect of surface active organic molecules (surfactants) in aqueous droplets and how these influence the cloud condensation nuclei (CCN) activity of particles. Surfactants are frequently observed in atmospheric aerosol, cloud and fog water samples (Faccini et al., 1999; Mochida et al., 2002; Cheng et al., 2004; Lin et al., 2010; Song et al., 2012), collectively comprising a significant fraction of the organic aerosol mass. For example, humic-like substances (HULIS) have been found to account for up to 60 % of water-soluble carbon in rural aerosols (Kiss et al., 2005).

Surface activity and how it is accounted for in the thermodynamic representation of aerosol water uptake has been found to significantly impact model predictions of CCN activity for some atmospheric organics (Prisle et al., 2008, 2010b). Introducing these predictions in large-scale atmospheric modelling of cloud–climate interactions and radiative forcing have been demonstrated to translate into impacts of comparable magnitude to the existing uncertainty in climate modelling (Prisle et al., 2012). Hence it is increasingly important to understand the effect of surface activity on cloud droplet activation; however, to this date only a limited number of organic aerosol systems have been characterized in terms of their surface activity.

The hygroscopicity parameter  $\kappa$  (kappa) was introduced by Petters and Kreidenweis (2007) as a single variable to account for chemical effects on aerosol water uptake in equilibrium Köhler predictions of droplet growth and cloud activation. The  $\kappa$  value is defined as an operational parameter and can be obtained from measurements of either hygroscopic water uptake in the subsaturated humidity regime or from the critical point of cloud droplet activation at supersaturated conditions, i.e. the critical particle diameter defined as the dry particle diameter, where 50 % of the particles can activate at a given supersaturation (SS). As an operationally defined parameter, the  $\kappa$  value can be seen as describing aerosol–water mixing interactions with respect to a volume-based reference state. As aerosol growth is a combined effect of water uptake properties of components within the aerosol mixture, a range of aerosol–water mixing states is spanned by the subsaturated and supersaturated measurements respectively (Prisle et al., 2010a). Provided that interactions of the mixture of individual aerosol components with water remain unchanged (or “ideal”, as defined with respect to a certain reference state) over the entire concentration range spanned by measurements, the  $\kappa$  value determined at different humidity, and at sub- and supersaturated conditions in particular, should remain unchanged. However, (non-ideal) mixing interactions of especially organic aerosol components with water are largely unknown and may be very complex, in particular in the presence of inorganics in the mixture (Prisle et al., 2010a). In general, previous studies comparing  $\kappa$  values at sub- and supersaturated conditions found that the subsat-

urated  $\kappa$  values were lower than supersaturated  $\kappa$  values for both ambient aerosols and laboratory-generated aerosols, especially in the case of secondary organic aerosol (Good et al., 2010; Massoli et al., 2010; Cerully et al., 2011; Dusek et al., 2011; Hersey et al., 2013; Hong et al., 2014; Pajunoja et al., 2015); however, a few studies found the discrepancy to be insignificant for some aerosol compositions and particle diameters (Good et al., 2010; Dusek et al., 2011).

Organosulfates (OSs, organic sulfate esters) have been observed as constituents of atmospheric aerosols in a wide range of environments, such as south-eastern USA (Surratt et al., 2008; Lin et al., 2012), northern Europe (Iinuma et al., 2007; Froyd et al., 2010; Kristensen and Glasius, 2011; Nguyen et al., 2014) and even the Arctic, where OSs have been found to comprise 7–15 % of total organic matter and 9–11 % of submicron organic matter in two independent studies (Frossard et al., 2011; Hansen et al., 2014). Some OSs derived from monoterpenes contain a hydrophobic carbon ring and may prefer to stay at the liquid/air interface in aqueous solutions (i.e. exhibit surface activity). Despite the apparent atmospheric abundance and widespread relevance of organosulfates, their cloud-forming properties have not yet been investigated; this gap has motivated the present study, where an atmospherically relevant organosulfate is characterized in terms of surface activity and hygroscopic properties.

Here, an OS derived from limonene with a molecular weight of 250 Da (L-OS 250) was synthesised. The hygroscopic properties of L-OS 250, ammonium sulfate (AS) and mixtures hereof were studied in the laboratory employing a unique custom-built set-up, allowing parallel measurements at sub- and supersaturated conditions. Furthermore the surface tension of aqueous solutions of L-OS 250 and L-OS 250 in mixtures with AS were measured.  $\kappa$  was derived from the measurements at sub- and supersaturated conditions as well as modelled based on the volume additive Zdanovskii–Stokes–Robinson (ZSR) mixing rule (Petters and Kreidenweis, 2007) and three different thermodynamic models, each employing a unique representation of surface activity and its effects on hygroscopic growth and cloud activation. The specific aims of the study are to investigate how  $\kappa$  is influenced by humidity, particle diameter and L-OS 250 / AS mixing ratio as well as to scrutinise whether the model representations can reproduce the experimental  $\kappa$  values for the system. The ability of the models to reproduce hygroscopicity measurements on the process level is very important for their further applicability in e.g. global climate models. Finally the study aims towards evaluating the cloud-forming properties of organosulfates.

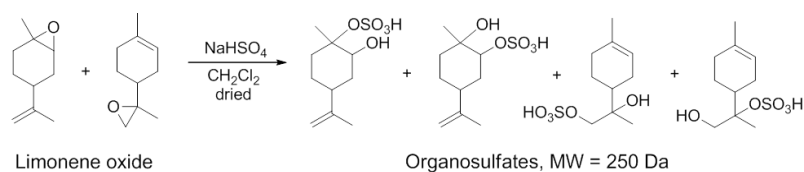


**Figure 1.** Synthesis of limonene-derived organosulfates with a molecular mass of 250 Da (L-OS 250) by ring opening of limonene epoxides with sodium hydrogen sulfate. The reaction is based on Cavdar and Saracolu (2009).

## 2 Methods

## 2.1 Synthesis of limonene-derived organosulfates

L-OS 250 isomers were synthesised using the method presented by Cavdar and Saracoğlu (2009) for synthesis of hydroxy sulfate esters by ring opening of epoxides with sodium hydrogen sulfate. Approximately 0.61 g limonene oxide was dissolved in 20 mL dried dichloromethane ( $\text{CH}_2\text{Cl}_2$ ). Next, 1.10 g dried sodium bisulfate ( $\text{NaHSO}_4$ ) was added to the reaction solution under magnetic stirring. The mixture was left at room temperature for 4–5 days for reaction, while the reaction environment was kept inert using nitrogen gas. The reaction scheme for the synthesis is given in Fig. 1.

Following synthesis, the product was purified by solid phase extraction on an ion exchange hydrophilic column (Strata-X-A 33u polymeric strong anion, Phenomenex) using a solvent sequence of 10 % acetonitrile in Milli-Q water followed by acetonitrile and chloroform.

Based on analysis using an ultra-high performance liquid chromatograph coupled to a quadrupole time-of-flight mass spectrometer through an electrospray ionisation inlet (UHPLC-ESI-q-TOF-MS) running in either positive or negative ionisation mode, it was estimated that an approximately 90 ( $\pm 5$ ) % pure sample of L-OS 250 isomers was obtained in the acetonitrile fraction, the 10 % impurities being by-products of organosulfates with MW 268 and MW 384 (chromatograms from the UHPLC-ESI-q-TOF-MS analysis are given in the Supplement).

## 2.2 Measurement of surface tension

Aqueous solutions of L-OS 250 and mixtures of L-OS 250 and AS (Sigma-Aldrich ≥ 99 %) were prepared in Milli-Q water (resistivity of 18.2 MΩ cm at 25 °C) for measurement of surface tension,  $\sigma$ . For each solute composition, nine or more solutions of different concentrations were made to obtain measurements over a broad concentration range (see details in Table 1).

Surface tension of each solution was measured with a FTÅ 125 pendant drop tensiometer, with an overall uncertainty of  $\pm 2\%$ . Measurements were done over a concentration range capturing the transition region of solution surface tension as it changes from the pure water value to the level of maximum obtainable surface tension reduction. Approx-

**Table 1.** Composition and concentration range of the solutions used for surface tension measurements

Composition [% wt / wt]		No. solutions	Concentration range [mol L <sup>-1</sup> ]	
L-OS 250	AS		L-OS 250	AS
100	0	12	0.0001–0.24	–
80	20	10	0.0001–0.20	0.00005–0.10
50	50	9	0.0001–0.10	0.0002–0.20
20	80	9	0.0001–0.05	0.0007–0.37
10	90	9	0.0001–0.05	0.0017–0.85
5	95	9	0.0001–0.07	0.0035–2.7

imately 40 pictures were taken of each pendant drop and the surface tension was calculated based on the pictures by the programme FTA32. The surface tension reported here resulted from analysis of three succeeding droplets, where the relative standard deviation of the surface tension did not exceed 1 %. According to Noziere et al. (2014) surface tension of a pendant drop is reduced over time until the minimum equilibrium surface tension is reached; hence surface tension was measured for a L-OS 250 and a L-OS 250 with 80 % AS solution ( $C(L\text{-}OS\ 250) = 0.005\ M$ ) over a 30 min time period. The surface tension was found to be stable after approximately 1 min, and the following measurements were thus initiated after 2 min.

Measured surface tension was parametrised as a function of ternary solution composition according to the equation previously used by Prisle et al. (2010b), here in the form

$$\sigma = \sigma_w - a \cdot R \cdot T \cdot \ln \left( 1 + \frac{C_{L-OS\,250}}{h} \right), \quad (1)$$

where  $\sigma_w$  is the surface tension of pure water,  $C_{L\text{-OS}250}$  is the aqueous molar concentration of L-OS 250,  $R$  is the universal gas constant in  $\text{J K}^{-1} \text{ mol}^{-1}$  and  $T$  is the temperature in Kelvin.  $a$  and  $b$  are the Szyskowski equation fitting parameters, which were fitted as dependent on solute mixing ratio as

$$a = a_1 + a_2 \cdot \frac{C_{\text{AS}}}{C_{\text{AS}} + C_{\text{L-OS250}}}, \quad (2)$$

**Table 2.** Solutions of L-OS 250, AS and mixtures hereof for measurement of hygroscopic growth factor and CCN activation.

Composition [% wt / wt]		Total solute concentration [g L <sup>-1</sup> ]
L-OS 250	AS	
100	0	0.21
90	10	0.21
80	20	0.20
50	50	0.22
20	80	0.19
0	100	0.25

$$b = b_1 + b_2 \cdot \frac{C_{\text{AS}}}{C_{\text{AS}} + C_{\text{L-OS 250}}}, \quad (3)$$

where  $C_{\text{AS}}$  is the molar concentration of AS. The values for  $a_1$ ,  $a_2$  and  $b_1$  and  $b_2$  are given in Sect. 3.1.

### 2.3 Parallel hygroscopicity tandem differential mobility analyser (H-TDMA)/cloud condensation nuclei counter (CCNC) measurements

To study the hygroscopic properties and the CCN activation of particulate L-OS 250 and their mixtures with AS, a unique laboratory set-up was custom built, enabling parallel measurements of both subsaturated water uptake and supersaturated cloud droplet activation for the same aerosol sample.

An atomizer (TOPAS ATM 220) was used to generate particles from aqueous solutions comprising L-OS 250 and AS in different relative mixing ratios. Each solution was prepared with de-ionised and purified water (resistivity of 18.2 MΩ cm at 25 °C). The solute compositions (relative L-OS 250 and AS mass fractions) and total solute concentrations ( $C$ , [g(solute)L(solution)<sup>-1</sup>]) are given in Table 2. Following atomisation, the aqueous aerosol was dried by passing through a diffusion dryer containing silica gel, resulting in a dry aerosol with relative humidity (RH) in the range 4–7 %. It is assumed that particles at this RH are essentially water free and, furthermore, that their dry compositions reflect the relative solute mass fractions of the respective atomised solutions. At this point, the flow of dry particles was split two ways for parallel measurements of water uptake ability with a H-TDMA and cloud droplet activation with a CCNC. A schematic of the water uptake characterisation set-up is shown in Fig. 2. Compressed air was applied after atomisation to dilute the particle concentration in order to prevent coagulation.

The hygroscopic growth factor (HGF) of the generated particles was studied with the fifth generation University of Helsinki volatility hygroscopicity tandem differential mobility analyser (VH-TDMA) (Hong et al., 2014), in which the volatility mode was deactivated so the instrument func-

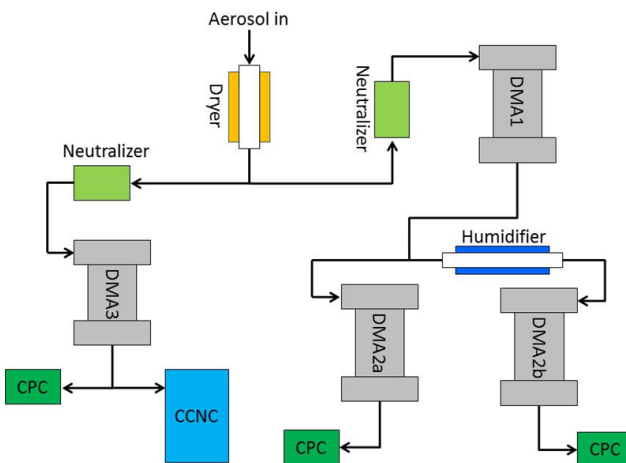


**Figure 2.** Schematic illustration of the experimental set-up for the dual H-TDMA and CCN measurements.

tions solely in hygroscopicity mode. The dry particles were charged by a neutraliser and passed through a differential mobility analyser (DMA1, Hauke type, see Fig. 2), in which a monodisperse aerosol distribution was selected based on the electrical mobility of the particles. For each particle composition, four individual dry diameters were selected: 30, 60, 100 and 145 nm. The flow of monodisperse particles was then split into two ways, one going into a humidifier and the other one bypassing the humidifier. The humidifier exposed the particles to an environment with four different set RHs of 80, 85, 90 and 93 %.

Number concentration size distribution data from both routines were measured using two similar systems, each including a differential mobility analyser (DMA2a and DMA2b, both Hauke type), scanning the size distribution of the particles, and a condensation particle counter (CPC, TSI 3010 and TSI 3772), counting the number concentration of particles.

The HGF of the particles at each RH was obtained as the ratio of the size distribution of the humidified ( $D_{\text{wet}}$ ) to dry ( $D_{\text{dry}}$ ) particles (Cruz and Pandis, 2000):

$$\text{HGF}(\text{RH}) = \frac{D_{\text{wet}}(\text{RH})}{D_{\text{dry}}}. \quad (4)$$

The H-TDMA was calibrated prior to the measurements using pure ammonium sulfate particles with diameters 30, 60, 100 and 145 nm at dry conditions. The obtained data in dry condition were used to calibrate the measured raw data at RHs in other regimes based on the algorithm introduced by Gysel et al. (2009). Furthermore, the measured growth factor distribution data were inverted using the piecewise linear inversion approach (Gysel et al., 2009) by the software Igor Pro to obtain the HGFs.

For each particle dry diameter, four to six measurements of the HGF were made at each RH and the relative standard deviation between these measurements was below 3 % for

all compositions. This standard deviation accounts for uncertainties related to the experimental set-up, including particle size selection and RH set point, as well as uncertainties connected with the data inversion process. Error bars presented in the following sections reflect the variation in measurements according to observed relative standard deviations ( $\pm 2$  standard deviation). The standard deviations found here are in line with a previous study, estimating uncertainties on HGFs to be below 5 % (Massling et al., 2009).

The ability of the generated particles to activate into cloud droplets at supersaturated conditions was measured with a CCNC from Droplet Measurement Technologies (DMT, model CCN-100) attached with a Hauke-type DMA (DMA3). After passing through a neutraliser, the dried particles were transferred to DMA3 (see Fig. 2), which scanned over the particle sizes. This means that the specific particle size selected in DMA3 was changed every second minute. The particle flow was then split into two lines, one going into a CPC (TSI, 3010), counting the total number concentration of particles, and one going to the CCNC, counting the number concentration of particles that activate or become droplets larger than  $1\text{ }\mu\text{m}$  at a given supersaturation. The nominal SS given by the CCNC was corrected to obtain the actual SS profile created in the instrument, based on measurements with AS following suggestions by Rose et al. (2008). Information regarding the calibration is given in the Supplement. CCN activation spectra were measured at thirteen different SSs, ranging from 0.099 to 0.922 % (calibrated values, corresponding to 100.099 to 100.922 % RH), by defining one supersaturation at the time and then scanning over the particle sizes (DMA3). The fraction of activated particles to total particles was thus obtained as a function of the particle dry diameter from the activation spectra. Activation spectra were corrected for multiply charged particles simultaneously selected in DMA3 and subsequently fitted using a sigmoidal function as done by Paramonov et al. (2013). From the fitted sigmoidal curve, the critical particle diameter ( $d_{50}$ ), was then determined.  $d_{50}$  for all SS was measured twice for all particle compositions except 90 % L-OS 250, for which SS was only measured once.

Regarding uncertainties on the measurements, it is estimated that the particle size selection in the DMA has an uncertainty of 3 % and based on previous studies it is estimated that the uncertainty on the SS in the CCNC after calibration has a maximum value of 5 % of SS (Rose et al., 2008; Asa-Awuku et al., 2009). Error bars presented in the following sections on critical particle diameter reflect these uncertainties.

#### 2.4 Calculation of $\kappa$

The critical particle diameters obtained from the CCN measurements and the HGFs obtained from the H-TDMA measurements were used to calculate an effective hygroscopicity parameter,  $\kappa$ , for all particle diameters, compositions and

humidity conditions. According to  $\kappa$ -Köhler theory, the  $\kappa$  parameter relates the dry diameter of particles of a specific chemical composition to the water uptake at a given RH or SS (Petters and Kreidenweis, 2007). Hence,  $\kappa$  primarily expresses the influence of chemical composition on water uptake.

From the HGF (H-TDMA experiment),  $\kappa$  was calculated by the equation (Hong et al., 2014):

$$S(D_{\text{wet}}) = \frac{\text{HGF}^3 - 1}{\text{HGF}^3 - (1 - \kappa)} \exp\left(\frac{4\sigma \text{MW}_w}{RT\rho_w D_{\text{dry}} \text{HGF}}\right), \quad (5)$$

where  $S(D_{\text{wet}})$  is the saturation ratio, equivalent to the RH set in the H-TDMA measurements, HGF is the hygroscopic growth factor obtained from H-mode measurements,  $D_{\text{dry}}$  is the particle dry diameter,  $\sigma$  is the droplet surface tension,  $\rho_w$  and  $\text{MW}_w$  are the density and molar mass of water respectively,  $R$  is the universal gas constant and  $T$  is the inlet temperature.

From the H-TDMA measurements  $\kappa$  can be calculated by inserting the experimental HGFs into Eq. (5) and then isolate  $\kappa$  by rearranging the equation.

For each dry particle diameter, RH and particle composition, HGF was measured four to six times, and hence four to six  $\kappa$  values were obtained. In the following sections  $\kappa$  for each composition at a given RH and dry particle diameter is represented as the mean  $\kappa$  values from these measurements. The standard deviation on the mean  $\kappa$  value was below 7 % for all compositions except for pure L-OS 250 where the standard deviation was up to 36 %. In the following sections error bars represent  $\pm 2$  standard deviations on the mean  $\kappa$ .

From the CCN measurements,  $\kappa$  was found using the equation:

$$S(D_{\text{wet}}) = \frac{D_{\text{wet}}^3 - D_{\text{dry}}^3}{D_{\text{wet}}^3 - D_{\text{dry}}^3 (1 - \kappa)} \exp\left(\frac{4\sigma \text{MW}_w}{RT\rho_w D_{\text{wet}}}\right), \quad (6)$$

where  $D_{\text{wet}}$  is the droplet diameter.

When the experimental critical particle diameter is inserted into Eq. (6) as  $D_{\text{dry}}$ ,  $\kappa$  can be iterated by varying the droplet diameter,  $D_{\text{wet}}$ , and  $\kappa$  itself until the minimum difference between the predicted supersaturation,  $S(D_{\text{wet}})$ , and the experimental supersaturation is obtained. Reported CCN  $\kappa$  values are thus the  $\kappa$  values resulting in minimum difference between the predicted and experimental supersaturation (Petters and Kreidenweis, 2007; Rose et al., 2010).

We calculate  $\kappa$  assuming the surface tension of pure water in Eqs. (5) and (6) above. The uncertainty on the CCN-derived  $\kappa$  values was estimated to 10 % (double the uncertainty on SS) and error bars on CCN-derived  $\kappa$  presented in the following sections represent this uncertainty.

Volume additive  $\kappa$  values were calculated for particles of mixed composition, based on the ZSR relation (Stokes and Robinson, 1966), by applying the mean measured  $\kappa$  values for pure AS and L-OS 250 according to their estimated re-

spective bulk volume fractions as previously done by for example Gysel et al. (2007), Petters and Kreidenweis (2007), Swietlicki et al. (2008) and Kristensen et al. (2014).

$$\kappa = \sum_i \varepsilon_i \kappa_i \quad (7)$$

Here,  $\varepsilon_i$  is the volume fraction of component  $i$  in the dry particle and  $\kappa_i$  is the intrinsic  $\kappa$  value for component  $i$  in its pure form. The volume fraction is calculated from the mass fraction and the density of each component. The bulk mass density of AS is well known as  $1.77 \text{ g cm}^{-3}$  but to the best of our knowledge the density of L-OS 250 is currently unknown. Ambient organic aerosol mass densities are generally observed to be between  $1.2$  and  $1.7 \text{ g cm}^{-3}$  (Hallquist et al., 2009) and a density of  $1.176 \text{ g cm}^{-3}$  was found for sodium dodecyl sulfate, SDS (Prisle et al., 2011, and references herein), a surfactant with a sodium sulfate group ( $\text{SO}_4\text{Na}$ ) considered to be similar to the sulfate group ( $\text{HSO}_4^-$ ) in organosulfates. Hence, here we calculate additive  $\kappa$  values assuming a density of  $1.176$  and  $1.7 \text{ g cm}^{-3}$  for L-OS 250 to cover this potential range. The volume additive  $\kappa$  values were calculated for the specific purpose of investigating the validity of the additivity assumption for calculating  $\kappa$  values for the L-OS 250/AS system.

## 2.5 Köhler modelling

Equilibrium growth by water uptake and cloud droplet activation was modelled for the studied particles using Köhler theory with three different model representations of organic surface activity, as previously introduced by Prisle et al. (2010b, 2011). Of these, in particular the bulk-to-surface partitioning model is a development of the model from Sorjamaa et al. (2004) and returns results similar to the model presented by Topping (2010) (e.g. Prisle et al., 2012).

The Köhler equation (Eq. 8) is analogous to Eqs. (5) and (6), but without the  $\kappa$  approach used to calculate water activity:

$$S(D_{\text{wet}}) = x_w \cdot \gamma_w \cdot \exp\left(\frac{4\sigma \text{MW}_w}{RT\rho_w D_{\text{wet}}}\right), \quad (8)$$

where  $x_w$  is the water mole fraction and  $\gamma_w$  is the corresponding activity coefficient of water, which is here set to unity. The dry particle diameter and composition and the droplet diameter are the input parameters, which means that HGF must be known; hence the equilibrium RH can be calculated. HGF is varied until equilibrium RH is equal to the experimental RH (80, 85, 90 or 93 %). Similarly, when the dry particle diameter and composition are the input parameters, critical supersaturation ( $\text{SS}_c$ ) can be solved numerically by varying the droplet diameter. In both cases, the droplet composition is assumed to be known and is used to calculate the droplet solution surface tension (Eq. 1). Here, the effects of bulk-to-surface partitioning on the resulting water mole fraction and solute concentrations used to calculate surface tension

can furthermore be accounted for. Alternatively, the surface tension can be fixed to the constant value for pure water.

Each model returns values of HGF and  $\text{SS}_c$  under different assumptions, which are used to calculate  $\kappa$  from Eqs. (5) and (6) respectively.

The three different model approaches were used to assess the effects of surface tension reduction and surfactant bulk-to-surface partitioning on the L-OS 250 water uptake. First, bulk-to-surface partitioning and surface tension effects are both ignored ( $\sigma_w$ ), which in particular means that the droplet surface tension in the Köhler equation is taken as that of pure water. Second, reduction of droplet surface tension from L-OS 250 is considered, but the influence of bulk-to-surface partitioning is still ignored ( $\sigma_b$ ), and thus bulk solution properties are assumed. This means using Eq. (8) with the concentration dependent surface tension (Eq. 1) according to the total droplet concentration of L-OS 250. Third, bulk-to-surface partitioning is considered in the evaluation of the droplet bulk phase composition and surface tension ( $\sigma_p$ ). This means that bulk solution concentrations used to calculate surface tension and water mole fraction change when the surfactant partitions to the droplet surface. Additional details about the surfactant partitioning calculations are given in the Supplement.

Droplet solution concentrations are calculated from the number of moles of each species (water, AS and L-OS 250), while assuming partial effective dissociation for ammonium sulfate ( $\nu \sim 2.3$  based on the parametrisation presented by Prisle, 2006) and no dissociation for L-OS 250 ( $\nu = 1$ ). Since L-OS 250 is a molecular species and expected to be a very weak acid it is assumed that L-OS 250 does not dissociate in solution but primarily is present in its molecular form. Both AS and L-OS 250 are assumed to be fully dissolved at all relevant droplet concentrations and droplet solutions are also assumed to be ideal with respect to water ( $\gamma_w = 1$  in Eq. 8) due to the current lack of explicit information on non-ideal solution interactions involving L-OS 250. A mass mean molecular weight of  $255.3 \text{ Da}$  was assumed for L-OS 250, based on the 10 % impurities (see Supplement). Since the droplet surface tension fit (Eq. 1) can give negative surface tension values at high L-OS 250 concentrations, the minimum surface tension has been limited to  $0.020 \text{ N m}^{-1}$ . In practice, this means that further bulk-to-surface partitioning cannot be calculated when this limit has been exceeded (see Supplement). This corresponds to the physical situation of constant surface tensions obtained for solutions above the so-called critical micelle concentration, where the aqueous surface is saturated in adsorbed surfactant and no further bulk-to-surface partitioning takes place (for more details, see Prisle et al., 2010b).

### 3 Results and discussion

#### 3.1 Surface tension

Figure 3 shows the surface tension of aqueous solutions of L-OS 250 and five mixtures of L-OS 250 and AS, as a function of the L-OS 250 molar concentration. L-OS 250 decreased the surface tension of aqueous solution from that of pure Milli-Q water ( $73 \text{ mN m}^{-1}$  at  $20^\circ\text{C}$ ) considerably. Even at a concentration of  $0.0025 \text{ mol L}^{-1}$  the surface tension was decreased to  $55.5 \text{ mN m}^{-1}$ . The surface tension further decreased to  $39.4 \text{ mN m}^{-1}$  when the L-OS 250 concentration increased to  $0.24 \text{ mol L}^{-1}$ . Surface tension of the mixed L-OS 250 and AS solutions with  $\leq 50\% \text{ w/w AS}$  converges towards the surface tension of pure aqueous L-OS 250, while the surface tension for the mixed solutions with  $\geq 80\% \text{ AS}$  was lower than for the solutions of pure L-OS 250 with the same aqueous concentration. Previous studies have shown that addition of AS to pure water increased the surface tension (Lee and Hildemann, 2013; Matubayasi, 2013); however, a decrease in surface tension of an organic solution when AS is added has been observed. For example, Ekström et al. (2009) found the surface tension of solutions of mannitol and methylerythritol to decrease with addition of  $17\% \text{ w/w AS}$ , whereas the surface tension of solutions of adipic acid and methylthreitol increased with the same mass addition of AS. The difference in surface tension of the individual organic solutions, when AS is added, can be explained by a difference in surface activity of the organics and a difference in interaction effects between AS and the organics. The additional surface tension reduction observed at high AS concentration in the present study is consistent with a salting out effect, where the presence of AS in solution decreases the solubility of L-OS 250, hereby forcing L-OS 250 towards the solution surface.

For the investigated system, the lowest surface tension was observed for the L-OS 250 solutions with 90 % AS at all L-OS 250 concentrations, where the surface tension dropped from approximately  $73$  to  $33 \text{ mN m}^{-1}$  over the concentration range of  $0.0001$  to  $0.05 \text{ mol L}^{-1}$  L-OS 250. Interestingly, the surface tensions of the L-OS 250 solutions with 95 % w/w AS were increased compared to the 90 % w/w AS of the same L-OS 250 concentration, over the full concentration range probed and converged towards the surface tension of pure L-OS 250 at concentrations lower than  $0.005 \text{ mol L}^{-1}$ . These observations suggest the presence of non-additive effects of L-OS 250 and AS affecting solution surface tension, since the surface tension at a given L-OS 250 concentration does not decrease monotonically with AS concentration over the full range of L-OS 250/AS mixing ratios from 100 to 0 % L-OS 250. At 90 % AS, salting out of the organic appears to be the dominant effect causing surface tension to decrease below the additive effects of each solute component separately in solution, whereas at 95 % AS the increase in surface

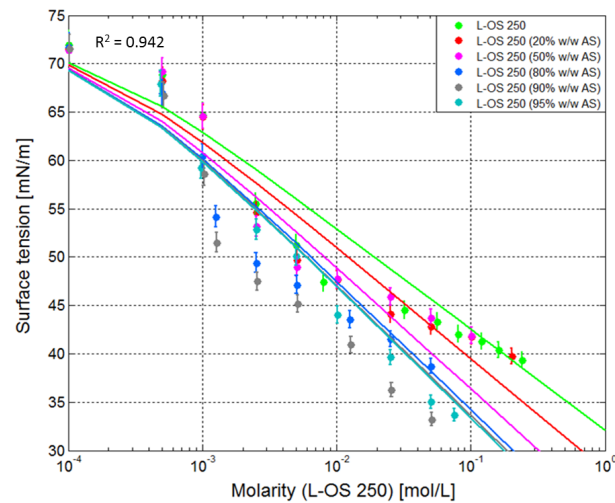


**Figure 3.** Surface tension as a function of the concentration of limonene organosulfate (L-OS 250) for six mixtures of L-OS 250 and ammonium sulfate (AS). Note that the data are plotted in semi-log space. Lines represent parametrisation curves and error bars show the 2 % instrumental uncertainty.

tension caused by AS is no longer fully counteracted by surfactant salting out.

Measured surface tensions were parametrised as a function of ternary solution composition according to Eq. (1). The fits are plotted in Fig. 3 together with measured data and the fitting parameters are  $a_1 = 1.86 \times 10^{-6} \text{ mol m}^{-2}$ ,  $a_2 = 5.78 \times 10^{-7} \text{ mol m}^{-2}$ ,  $b_1 = 1.30 \times 10^{-4} \text{ mol L}^{-1}$ ,  $b_2 = 1.67 \times 10^{-6} \text{ mol L}^{-1}$ . From Fig. 3 it is evident that there are some L-OS 250 molarity regions with slightly different surface tension slopes, which cannot be captured by the simple surface tension fit. This is true for all solution compositions and is most likely caused by the impurities in L-OS 250. Furthermore the fit has difficulties capturing the composition-dependent surface tension variation, indicating that the combined influences of L-OS 250 and AS on ternary aqueous surface tension are not linearly additive, as is also clear from the trend in the measurements. This might be expected for two components of very different molecular structures and behaviour in respective binary aqueous solutions.

#### 3.2 Hygroscopic growth factor

Figure 4 shows HGF of laboratory generated particles of L-OS 250, AS and their mixtures as a function of RH. The HGF is shown for particles of four dry diameters ( $30$ ,  $60$ ,  $100$  and  $145 \text{ nm}$ ) being exposed to  $80$ – $93\% \text{ RH}$ .

All six particle compositions showed hygroscopic growth at the selected RHs, and the HGF increased with increasing RH in each case, as expected for particles with non-vanishing hygroscopicity.

Only weak hygroscopic growth was observed for the pure L-OS 250 particles with HGF increasing from approximately

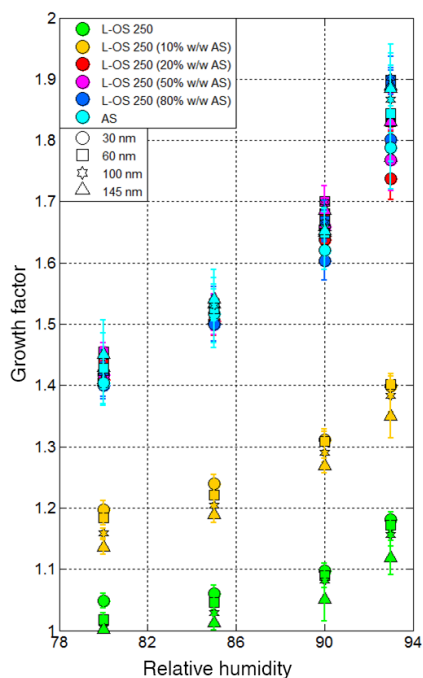


**Figure 4.** Hygroscopic growth factor (HGF) as a function of relative humidity (RH) for particles of pure L-OS 250, pure AS and mixtures hereof. Growth factor is given for four dry particle diameters of each chemical composition. Each data point represents the mean HGF obtained from four to six measurements, and the error bars express  $\pm 2$  standard deviations as described in Sect. 2.3.

1.0 (no growth) at 80 % RH to 1.2 at 93 % RH, where the water uptake occurs smoothly over the given RH range. No deliquescence is observed for L-OS 250 in the monitored RH range but since the hygroscopic growth occurs smoothly, deliquescence activation at supersaturation, as previously observed for some insoluble or slightly soluble organics (Kreidenweis et al., 2006), is not expected. To the best of our knowledge the aqueous solubility of L-OS 250 is currently not characterized but the presented data are consistent with a modest L-OS 250 solubility, leading to a saturated solution with a water activity of about 0.85 at the onset of hygroscopic growth. The HGF of pure AS particles on the other hand increased from approximately 1.4 to 1.9 over the same RH range, consistent with the well-documented hygroscopic properties and deliquescence RH of AS of 79.9 ( $\pm 0.5$ ) % at 295 K (Seinfeld and Pandis, 2006).

For the mixed particles, the HGF corresponding to a given dry particle diameter and RH increased with increasing weight percentage of AS, in accordance with an increasing contribution of the more hygroscopic component. For mixtures with  $\geq 20$  % w / w AS, the overall HGF converged towards the HGF of pure AS for all particle diameters; thus the system shows a non-linear composition dependency in HGF. It must be kept in mind that when a particle with presumably 80 % w / w of L-OS 250 or some other organic demonstrates

the same HGF as a pure AS particle, it does not imply that the organic has no intrinsic hygroscopicity in the mixture but rather that the resulting impact of the organic in the mixed particle is similar to the hygroscopic properties that would arise from the same particle fraction being composed purely of AS. In accordance with Köhler theory, any reduction of droplet surface tension from L-OS 250 should increase effective particle hygroscopicity. This means that surface tension effects of L-OS 250 in our experiments appear to compensate for a possible decrease in direct impact on water activity from the larger molecular size, lower solubility and lower dissociation degree of L-OS 250 compared to AS.

Non-linear composition dependency has previously been observed for the hygroscopicity of particles of mixed organic and inorganic compounds. Hämeri et al. (2002) found an overall particle hygroscopicity close to that of pure AS when measuring the HGF for particles of malonic acid and succinic acid with 50 % w / w AS. In our experiments the non-linear composition dependency is more pronounced as HGF values of the mixed particles already coincide with the ones for pure AS at as low as 20 % w / w AS which could be caused by differences in surface activity of the organic compounds and their interaction with AS. For example, the acids considered by Hämeri et al. (2002) are hygroscopic and only weakly surface active in contrast to L-OS 250 showing significant surface activity, pointing to the significance of surface tension reduction effects for increasing the organic contribution to particle hygroscopicity. It should be mentioned that the dry particle compositions in these experiments are assumed to reflect the solute compositions of the original aqueous solutions from which they are generated. It has previously been suggested that deviations in the particle composition can occur through processes such as bulk-to-surface partitioning or micelle formation in the atomizer or the generated droplets. However, it is our firm belief that such processes would increase the amount of L-OS 250 in the particles, not decrease it; hence these processes cannot explain the non-linear composition dependency towards the hygroscopic properties of AS observed.

In general, the dry diameter of the particles was observed to have little or modest influence on the measured HGF; however, for the particles of pure L-OS 250 and L-OS 250 with 10 % w / w AS, the largest HGF was observed for the smallest particle diameters compared with the larger particles. For the pure AS particles and particles with  $\geq 20$  % w / w AS, the opposite behaviour was seen, where the largest HGFs were measured for the largest particles. This further supports our inferences related to effects of organic solubility vs. surface activity: for particles with the highest fractions of L-OS 250, there could be kinetic effects of dissolution present, increasing the amount of dissolved material in the smallest particles, compared to the larger ones. Conversely, for particles with larger amounts of AS relative to L-OS 250, the hygroscopicity of the inorganic likely negates any effects of limited organic solubility. For these particles the dependence on dry

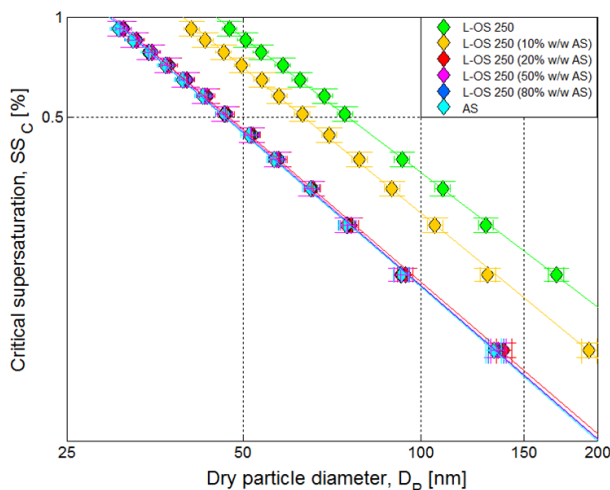


**Figure 5.** Critical supersaturation ( $SS_c$ ) as function of dry particle diameter for the six investigated particle compositions. The curves follow the Köhler slope of approximately  $-3/2$  for L-OS 250/AS compositions with  $\geq 20\%$  AS. The curves for pure L-OS 250 and L-OS 250 with 10 % AS have a slope of approximately  $-1.4$ . Error bars represent the uncertainty on the particle dry size diameter ( $x$  axis) and  $SS_c$  ( $y$  axis). Note that the data are plotted in log–log space.

diameter may be related to effects of organic depletion from bulk-to-surface partitioning, decreasing the relative amount of hygroscopic material in the droplet bulk of the smallest particles, compared to the larger ones (Prisle et al., 2010b).

### 3.3 Critical particle diameter

Figure 5 shows the  $SS_c$  as function of the dry particle diameter ( $D_{dry}$ ) for the six different dry particle compositions studied. The ( $D_{dry}$ ,  $SS_c$ ) pairs have been adopted here from the measured d<sub>50</sub> values at each SS. Unfortunately measurements at SS 0.099 and 0.442 % resulted in negative values of the dry diameters for the pure L-OS 250 particles; hence these data points are not present here.

Particles of all compositions could activate into cloud droplets in the investigated SS range and the  $SS_c$  for activation decreased with increasing dry particle diameter as expected from equilibrium Köhler theory. Pure L-OS 250 particles activated at larger dry diameters than particles of pure AS at all selected SS: for example at a SS of 0.16 % pure L-OS 250 activated at a dry diameter of 170 nm, whereas AS activated at a dry diameter of 93 nm. The curves for all six compositions have slopes close to the Köhler slope of approximately  $-3/2$  in log–log space. According to equilibrium Köhler theory a slope of  $-3/2$  means that no explicit size-dependent effects are present in the obtained CCN spectra (Seinfeld and Pandis, 2006). Pure AS and L-OS 250 with 80, 50 and 20 % w / w AS had a slope of  $-3/2$ , while the slope for pure L-OS 250 and L-OS 250 with 10 % w / w

AS were numerically slightly smaller (approximately  $-1.4$ ), consistent with the presence of a modest size dependent effect attributed to L-OS 250.

As was also observed for the measured subsaturated HGF, supersaturated activation properties of the mixed particles were dominated by AS, where the critical particle diameter at all SSs decreased with increasing weight percentage of AS. For particles with  $\geq 20\%$  w / w AS the critical particle diameter is essentially the same as for pure AS.

Previous studies of mixed organic and inorganic particles showed similar observations of a decrease in critical particle diameter with increasing amount of inorganics. For example, Prisle et al. (2010b) found the critical particle diameters of mixed surfactant (e.g. sodium octanoate, sodium decanoate, sodium dodecanoate and sodium dodecyl sulfate) and sodium chloride (NaCl) particles to decrease with increasing NaCl mass fraction in the particles, when investigating surfactant/NaCl systems with 5 to 80 % w / w NaCl. However, in contrast to the present study, the critical particle diameters did not coincide for any of the different surfactant/NaCl compositions investigated, indicating that the full cancellation of different opposing effects did not occur in their study.

### 3.4 $\kappa$ values

$\kappa$  values were calculated based on the H-TDMA measurements using Eq. (5) and based on the CCN measurements using Eq. (6) as well as using the ZSR-based additive formula (Eq. 7). Furthermore, CCN experiments were modelled from equilibrium Köhler theory employing three different sets of assumptions, as explained in Sect. 2.5, and the corresponding  $\kappa$  values were calculated from the modelled critical supersaturations using Eq. (6).

#### 3.4.1 H-TDMA-derived $\kappa$

Figure 6 shows  $\kappa_{H-TDMA}$  as function of RH and dry particle diameter ( $D_{dry}$ ) for the six compositions of L-OS 250 mixed with AS investigated. The obtained  $\kappa$  values for particles of all six chemical compositions at the four RHs showed a consistent dependency on dry diameter, where  $\kappa$  decreased with increasing particle diameter. The error bars, here representing  $\pm 2$  standard deviations, on individual  $\kappa$  values for a given composition show some overlap for the high AS fraction composition, whereas no overlap is observed for pure L-OS 250 and L-OS 250 with 10 % w / w AS, suggesting that this trend may be statistically significant for at least the latter two. To our knowledge, this is the first time that a decrease in  $\kappa_{H-TDMA}$  with increasing dry particle diameter has been reported for particles of the same chemical composition.

Some studies of ambient aerosols have on the contrary shown that  $\kappa$  values increase with particle diameter. For example, Holmgren et al. (2014) and Wu et al. (2013) found  $\kappa_{H-TDMA}$  to increase with particle diameter during field cam-

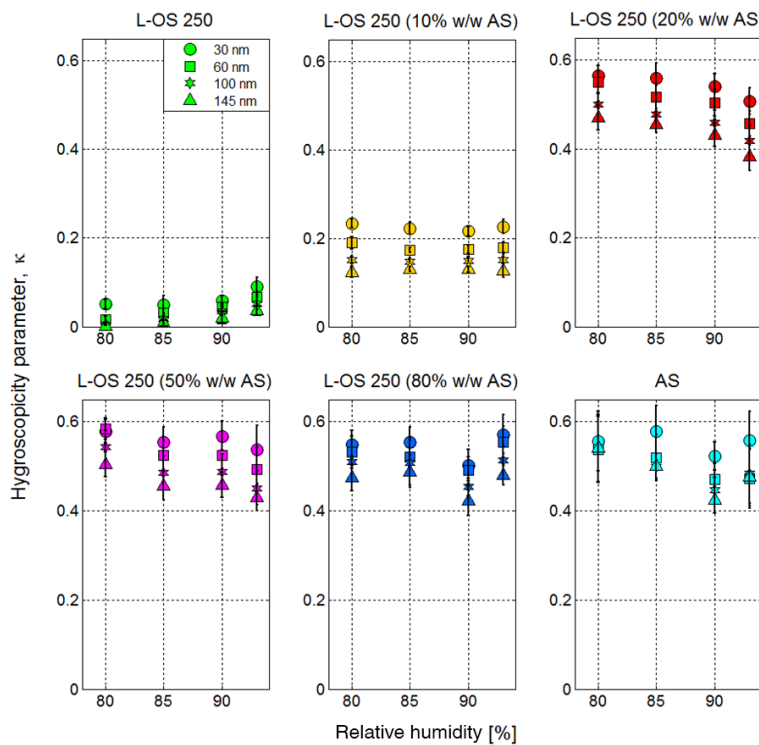


**Figure 6.** Hygroscopicity parameter,  $\kappa$ , obtained from the H-TDMA measurements, as a function of RH for the six mixtures of L-OS 250 and AS. Error bars represent  $\pm 2$  standard deviations on  $\kappa$  as described in Sect. 2.4.

paigns in France and Germany respectively. However, for field measurements the chemical composition of the particles with all likelihood changes with particle diameter and with time; hence the change in  $\kappa$  observed with increasing particle diameter in the field studies is probably a result of changing chemical composition. In this study, particles of different diameters were formed from atomisation of the same solution; hence, ideally they should have the same chemical composition. If this is the case, then the observed trend implies that the smaller particles are more hygroscopic than larger ones of the same chemical composition. An actual size dependency for invariant particle composition could result from changes in surface effects or dissolution kinetics with particle size. It should be mentioned that the observed size dependency could potentially be an indirect effect of a changing chemical composition or from an artefact in our experiments. From the HGF measurements, a bimodal humidified size distribution (with one dominating and one satellite mode) was observed for the mixed L-OS 250/AS particles, indicating that the particles may be somewhat externally mixed; thus it is possible that droplets formed with the atomizer from mixed L-OS 250/AS solutions have different chemical composition due to the surface activity of L-OS 250. The same could in principle be true for the pure L-OS 250 particles, since approximately 10 % impurities (of two other organosulfates) were present here; these impurities are very similar in structure to L-OS 250. However, it cannot explain the observed

size dependency of the pure AS particles which should be fully soluble and not surface active in any case. We therefore do not believe that changing particle composition is the main cause of the observed particle size dependency of  $\kappa_{\text{H-TDMA}}$ . Based on the relatively modest size dependency observed from our results, we cannot give the conclusive statement that smaller particles are more hygroscopic than larger ones of the same chemical composition. However, the results present the possibility and further studies should be conducted to confirm this.

Regarding RH,  $\kappa_{\text{H-TDMA}}$  for pure L-OS 250 increased significantly ( $\kappa/\kappa_{93\% \text{ RH}} \cdot 100\% = 44, 72, 92$  and 95 % for 30, 60, 100 and 145 nm particles respectively), when RH increased from 80 to 93% humidity. This increase in  $\kappa_{\text{H-TDMA}}$  could be caused by increased dissolution of L-OS 250. At low RH (here 80 %), the water content in the droplets may not be high enough to dissolve the L-OS 250 particle entirely, resulting in a mixed liquid- and solid-phase droplet. Both Henning et al. (2012) and Zardini et al. (2008) have previously suggested that phase separation could make aerosol hygroscopicity RH dependent and Henning et al. (2012) found that soot particles coated with solid succinic acid resulted in no hygroscopic growth whereas soot particles coated with liquid/dissolved succinic acid resulted in hygroscopic growth, suggesting that the increase in  $\kappa_{\text{H-TDMA}}$  observed here could also be caused by gradual dissolution of

L-OS 250 with increasing RH. This effect will be discussed further in Sect. 3.4.3.

For the pure AS particles and the L-OS 250 particles with 10, 50 and 80 % w / w AS, increasing subsaturated RH showed no clear effect on  $\kappa_{\text{H-TDMA}}$ . For these compositions, the  $\kappa_{\text{H-TDMA}}$  appeared to be within a stable range, independent of RH. For L-OS 250 particles with 20 % w / w AS,  $\kappa_{\text{H-TDMA}}$  decreased with increasing RH. This changing behaviour of  $\kappa$  with respect to RH for the different particle compositions may be due to a change in interactions between AS and L-OS 250 with changing mass fraction, which could influence the particle water activity.

$\kappa_{\text{H-TDMA}}$  showed a clear increase with increasing mass fraction of AS, where  $\kappa_{\text{H-TDMA}}$  for mixtures with  $\geq 20$  % AS converged towards the values of pure AS. As discussed by Sjogren et al. (2008), interaction of inorganic and organic species can increase the overall particle hygroscopicity and thus the apparent hygroscopicity of organic compounds; hence the high  $\kappa$  values observed for the mixed particles with  $\geq 20$  % w / w AS, which cannot be explained by increasing AS fraction alone, are expected to be a result of such interactions. The  $\kappa_{\text{H-TDMA}}$  for pure L-OS 250 (0.002 to 0.09) correspond to weakly hygroscopic organic compounds according to Petters and Kreidenweis (2007). L-OS 250 contains an alcohol group and a sulfate group, which are both polar; however, the molecule contains a hydrophobic ring structure, and hence it is not surprising that the hygroscopicity of L-OS 250 is modest. The  $\kappa_{\text{H-TDMA}}$  for pure AS was here measured to be between 0.42 and 0.58, in line with previous studies, where  $\kappa$  for AS is in the range of 0.33 to 0.72 (Clegg et al., 1998; Koehler et al., 2006; Carrico et al., 2008).

#### 3.4.2 CCN-derived $\kappa$

Figure 7 shows the CCN-derived  $\kappa$  values as a function of  $\text{SS}_c$  for the different particle compositions. In general,  $\kappa_{\text{CCN}}$  increased with increasing mass fraction of AS, and particles with  $\geq 20$  % w / w AS have  $\kappa$  values converging towards those of pure AS, exactly as was also found for  $\kappa_{\text{H-TDMA}}$ . This trend is therefore consistent over the whole humidity range investigated.  $\kappa_{\text{CCN}}$  for the pure L-OS 250 particles showed a weak increase with SS, implying a corresponding decrease of  $\kappa$  with increasing particle diameter, as the larger particles of a given composition activate at lower supersaturation conditions. However, contrary to the subsaturated conditions, particles of equivalent composition do not necessarily have the same dilution state when they activate at different supersaturations (Prisle et al., 2011). Supersaturated  $\kappa$  values are therefore not immediately comparable across different dry particle diameters.  $\kappa_{\text{CCN}}$  increased from 0.095 to 0.145 when the SSs increased from 0.168 to 0.922 %, corresponding to particle diameters 170 and 47 nm respectively (see Fig. 7).  $\kappa_{\text{CCN}}$  for the L-OS 250 particles with 10 % w / w AS also show a weak increase with SS, rising from 0.18 to 0.23 over the selected SS range. However, including the un-

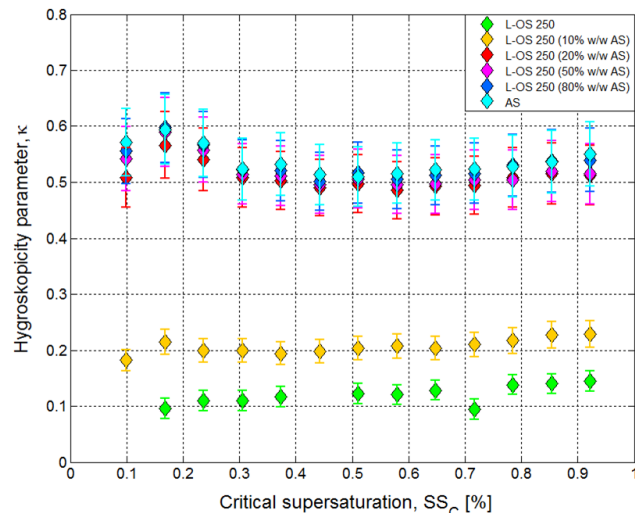


**Figure 7.** Hygroscopicity parameter,  $\kappa$ , derived from the CCN measurements, as a function of  $\text{SS}_c$  for six mixtures of L-OS 250 and AS. Error bars represent an estimated uncertainty of 10 % on  $\kappa$  and uncertainty on the  $\text{SS}_c$  is estimated to be 5 % / % as described in Sect. 2.4.

certainty on  $\kappa_{\text{CCN}}$ , the increasing trend for L-OS 250 and L-OS 250 with 10 % w / w AS is likely not significant. For the pure AS particles and the particles with  $\geq 20$  % w / w AS,  $\kappa_{\text{CCN}}$  showed no clear sign of increasing or decreasing trend with SS but fluctuated within a range for each particle composition (0.49 to 0.57 for L-OS 250 with 20 % w / w AS, 0.50 to 0.59 for L-OS 250 with 50 % w / w AS, 0.50 to 0.60 for L-OS 250 with 80 % w / w AS and 0.51 to 0.59 for pure AS), where the individual  $\kappa_{\text{CCN}}$  fell within the uncertainty range of each other. Since the size dependency is strongest for pure L-OS 250, this suggests relation to properties of the organic, such as dilution and/or surface activity effects. As  $\kappa$  for pure L-OS 250 decreases with increasing dry particle diameter and corresponding dilution state at activation, this suggests that decreasing surface tension may play a greater role for the smaller particles compared to surface partitioning, which is the opposite to what was observed for SDS in some cases by Sorjamaa et al. (2004). We argue that a mean  $\kappa_{\text{CCN}}$  for each particle composition can be used to represent  $\kappa_{\text{CCN}}$  over the entire SS range of 0.099–0.922 % investigated, as the individual  $\kappa_{\text{CCN}}$  fall within the overall uncertainty, and since the Köhler slopes obtained from the  $\text{SS}_c$  curves are approximately  $-3/2$  for all particle compositions, indicating the absence of significant size-dependent effects on  $\text{SS}_c$ . Hence, in the following,  $\kappa_{\text{CCN}}$  for each composition is given as the mean  $\kappa_{\text{CCN}}$  ( $\pm 1$  standard deviation) over the investigated SS range. In Table 3, the mean, minimum and maximum  $\kappa_{\text{CCN}}$  as well as standard deviation of  $\kappa_{\text{CCN}}$  is given.

**Table 3.** Mean, minimum and maximum values of the hygroscopicity parameter,  $\kappa$ , obtained from the CCN measurements, as well as standard deviations (SD).

	$\kappa_{\text{CCN}}$			
	Mean	SD	Minimum	Maximum
L-OS 250	0.120	0.017	0.095	0.145
L-OS 250 (10 % w / w AS)	0.207	0.013	0.182	0.229
L-OS 250 (20 % w / w AS)	0.510	0.022	0.486	0.566
L-OS 250 (50 % w / w AS)	0.519	0.028	0.496	0.589
L-OS 250 (80 % w / w AS)	0.532	0.027	0.501	0.597
AS	0.538	0.026	0.509	0.594

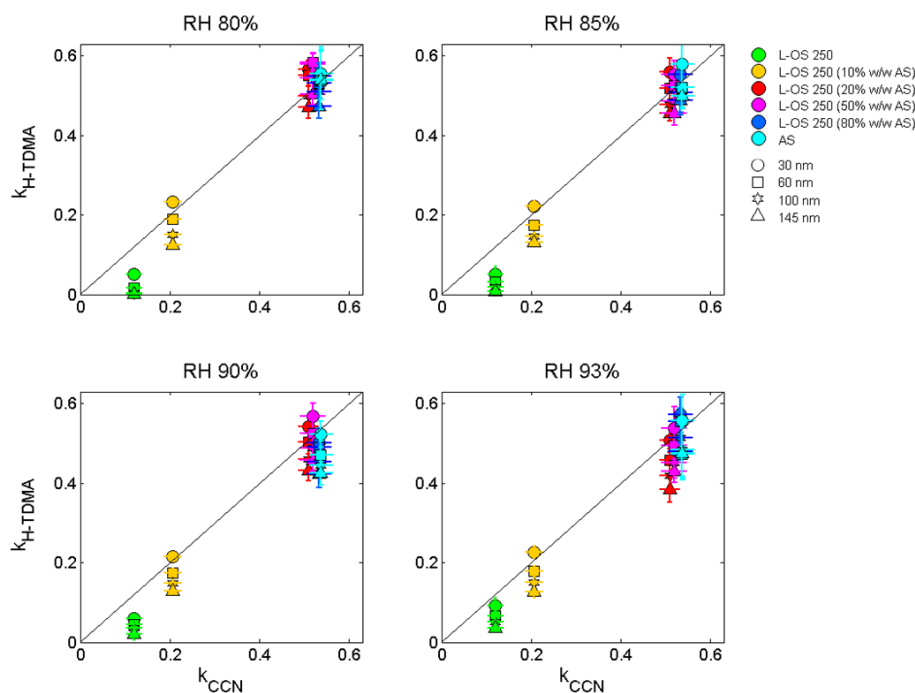


**Figure 8.** Hygroscopicity parameter,  $\kappa$ , derived from the H-TDMA measurements, plotted against  $\kappa$  obtained from the CCN measurements, for six mixtures of L-OS 250 and AS. A mean  $\kappa$  value for each composition was found for the CCN-derived  $\kappa$  and error bars denote the experimental uncertainty as explained in Sect. 2.4.

### 3.4.3 Comparison of H-TDMA- and CCN-derived $\kappa$

Comparing  $\kappa_{\text{H-TDMA}}$  and  $\kappa_{\text{CCN}}$  of each of the six particle compositions (see Fig. 8), it is clear that  $\kappa$  values for pure L-OS 250 (green markers) are higher for supersaturated (CCN) than for subsaturated (H-TDMA) conditions. This is observed for all RH and particle dry diameters measured with the H-TDMA. We note that the difference in  $\kappa$  between the two methods became smaller with increasing RH, meaning that at higher RH,  $\kappa_{\text{H-TDMA}}$  for L-OS 250 approach  $\kappa_{\text{CCN}}$ , as expected if there is indeed a dissolution effect present. As mentioned in Sect. 3.4.1, the increase in  $\kappa_{\text{H-TDMA}}$  for L-OS 250 with increasing RH could be caused by increased dissolution of L-OS 250, which would be consistent with the indications of its modest water solubility mentioned above.

This explanation is supported by the observation of  $\kappa_{\text{H-TDMA}}$  approaching  $\kappa_{\text{CCN}}$  with increasing RH. It is therefore suggested that the low  $\kappa_{\text{H-TDMA}}$  for L-OS at 80, 85 and 90 % RH is caused by incomplete dissolution of L-OS 250 resulting in a mixed solid-/aqueous-phase system.

The  $\kappa_{\text{H-TDMA}}$  for L-OS 250 with 10 % AS (yellow markers) coincide with  $\kappa_{\text{CCN}}$  for 30 and 60 nm particles whereas 100 and 145 nm particles have  $\kappa$  values below the corresponding  $\kappa_{\text{CCN}}$ . For L-OS 250 particles with  $\geq 20$  % w / w AS, it was generally observed that  $\kappa_{\text{H-TDMA}}$  for 30 nm particles were a bit higher than  $\kappa_{\text{CCN}}$ , whereas  $\kappa_{\text{H-TDMA}}$  for 145 nm particles were lower than  $\kappa_{\text{CCN}}$  and finally  $\kappa_{\text{H-TDMA}}$  for 60 and 100 nm particles were essentially the same as the obtained  $\kappa_{\text{CCN}}$ . An exception is found for pure AS at 90 % RH, and L-OS 250 with 20 to 80 % w / w AS at

93 % RH, where  $\kappa_{\text{H-TDMA}}$  was below  $\kappa_{\text{CCN}}$  for the three larger particle sizes. This is likely due to increased dissociation of AS with greater dilution (Prisle, 2006), as experienced for the larger particles at activation.

The trend of  $\kappa_{\text{H-TDMA}}$  being smaller than  $\kappa_{\text{CCN}}$  has previously been observed in other laboratory studies investigating secondary organic aerosol hygroscopicity (Prenni et al., 2007; Petters et al., 2009; Massoli et al., 2010; Wex et al., 2010; Pajunoja et al., 2015), as well as in field measurements of ambient aerosol (Cerully et al., 2011; Hersey et al., 2013; Hong et al., 2014). The discrepancies between  $\kappa_{\text{H-TDMA}}$  and  $\kappa_{\text{CCN}}$  found in the field studies were discussed by Hong et al. (2014), outlining different effects that could influence  $\kappa$ : first, the different degrees of dissolution of organics at sub- and supersaturated conditions, as well as potential phase separation of the particle; second, the difference in instrumental design of the H-TDMA and CCNC, such as the residence time in the humidifying unit of the instruments relative to the aerosol equilibration time at sub- and supersaturated conditions. In the set-up used here residence times in the humidifying units were assessed to 1 s in the H-TDMA and 10 s in the CCNC.

The difference between  $\kappa_{\text{H-TDMA}}$  and  $\kappa_{\text{CCN}}$  observed here can primarily be explained from the first-mentioned dissolution effect, since the discrepancy is mainly observed for the pure L-OS 250 particles, whereas the L-OS 250 particles with  $\geq 20$  % w / w AS in general had the same  $\kappa$  values measured in the two saturation regimes; hence the overall effect of interactions between AS and L-OS 250 are similar at sub- and supersaturation conditions at  $\geq 20$  % w / w AS. Close agreement between  $\kappa_{\text{H-TDMA}}$  and  $\kappa_{\text{CCN}}$  have previously been found for ambient aerosols with high mass fraction of ammonium and sulfate ions (e.g. Good et al., 2010). This could imply that a given amount of organics in aerosols may influence the aerosol hygroscopicity to a different extent at sub- and supersaturated conditions and that application of a single  $\kappa$  value for a specific aerosol chemical composition many not be sufficient for describing particle hygroscopicity over the entire sub- and supersaturated humidity range.

#### 3.4.4 $\kappa$ from modelled HGF and critical supersaturation

HGF and  $\text{SS}_c$  values for L-OS 250, AS and the four mixtures hereof were modelled from equilibrium Köhler theory employing three different assumptions concerning surface tension and bulk-to-surface partitioning. These assumptions are briefly summarised as follows.

1. Bulk-to-surface partitioning and surface tension effects are both ignored ( $\sigma_w$ ).
2. Reduction of surface tension from the organic is considered, but effects of bulk-to-surface partitioning on droplet concentration are ignored ( $\sigma_b$ ).

3. Bulk-to-surface partitioning is considered in the evaluation of the droplet bulk phase composition, and the impact on surface tension according to the resulting bulk concentrations is included ( $\sigma_p$ ).

From the modelled HGF and  $\text{SS}_c$  values,  $\kappa$  was calculated using Eqs. (5) and (6) respectively. The purpose is to examine if any of the three thermodynamic models can reproduce the observed hygroscopic behaviour for the investigated L-OS 250 containing particles. Furthermore,  $\kappa$  values for the four L-OS 250/AS mixtures were modelled using the volume additive ZSR mixing rule (Eq. 7), from the measured mean  $\kappa$  values of pure L-OS 250 and pure AS and the respective volume fractions of the two compounds. To obtain particle volume fractions from experimental mass fractions, we ideally need the actual mixed particle density, which is here estimated as the volume additive bulk mass density of different particle components. The density of L-OS 250 ( $\rho_{\text{L-OS 250}}$ ) is to the best of our knowledge unknown; hence the calculation was done using two different density cases for L-OS 250, 1.176 and 1.7 g cm<sup>-3</sup>, as explained in Sect. 2.4.  $\kappa$  was modelled this way for both sub- and supersaturated conditions.

Figure 9 shows the  $\kappa$  values resulting from the different model assumptions. The upper left panel shows the additivity representation of  $\kappa$  ( $\kappa_{\text{ZSR}}$ ) together with the measured values of  $\kappa_{\text{H-TDMA}}$  and  $\kappa_{\text{CCN}}$ .  $\kappa_{\text{ZSR}}$  calculated using  $\rho_{\text{L-OS 250}} = 1.176$  g cm<sup>-3</sup> ( $\kappa_{\text{ZSR}_1}$ ) resulted in  $\kappa$  values closer to the measured values than did  $\kappa_{\text{ZSR}}$  calculated using  $\rho_{\text{L-OS 250}} = 1.7$  g cm<sup>-3</sup> ( $\kappa_{\text{ZSR}_2}$ ) for all L-OS 250/AS compositions.  $\kappa_{\text{ZSR}_1}$  for L-OS 250 with 10 % w / w AS and 80 % w / w AS were reasonably close ( $\pm 10$  %) to  $\kappa_{\text{H-TDMA}}$  for 145 nm particles and  $\kappa_{\text{CCN}}$ ; however, for L-OS 250 with 20 and 50 % w / w AS,  $\kappa_{\text{H-TDMA}}$  and  $\kappa_{\text{CCN}}$  fall in the range of 0.4–0.6, whereas  $\kappa_{\text{ZSR}_1}$  have values of 0.17 and 0.32 for H-TDMA and 0.23 and 0.37 for CCN respectively. For these compositions, the additivity formula thus yields a very poor representation of the variations in measured  $\kappa$  values, suggesting that the additivity formula should only be used for compositions very close to either pure L-OS 250 or pure AS.

From Fig. 9 it is clear that the models  $\sigma_w$ ,  $\sigma_b$  and  $\sigma_p$  results in similar  $\kappa$  values in the subsaturated regime and that the values are practically independent of dry particle diameter and humidity. This behaviour is seen because surface tension changes have a negligible effect on the equilibrium RH, and the effects of surfactant bulk-to-surface partitioning is limited due to the higher droplet concentrations and lower surface-area-to-volume ratio for droplets conditioned at subsaturated humidity compared to supersaturated activation. As a result, the  $\kappa$  values from the Köhler representations are similar to the ZSR  $\kappa$  values and equally poor in representing the observed non-linear weight fraction dependency. This suggests that the non-linear composition dependency could be caused by dissolution and non-ideal internal droplet mixing interaction effects of L-OS 250, which are not accounted for

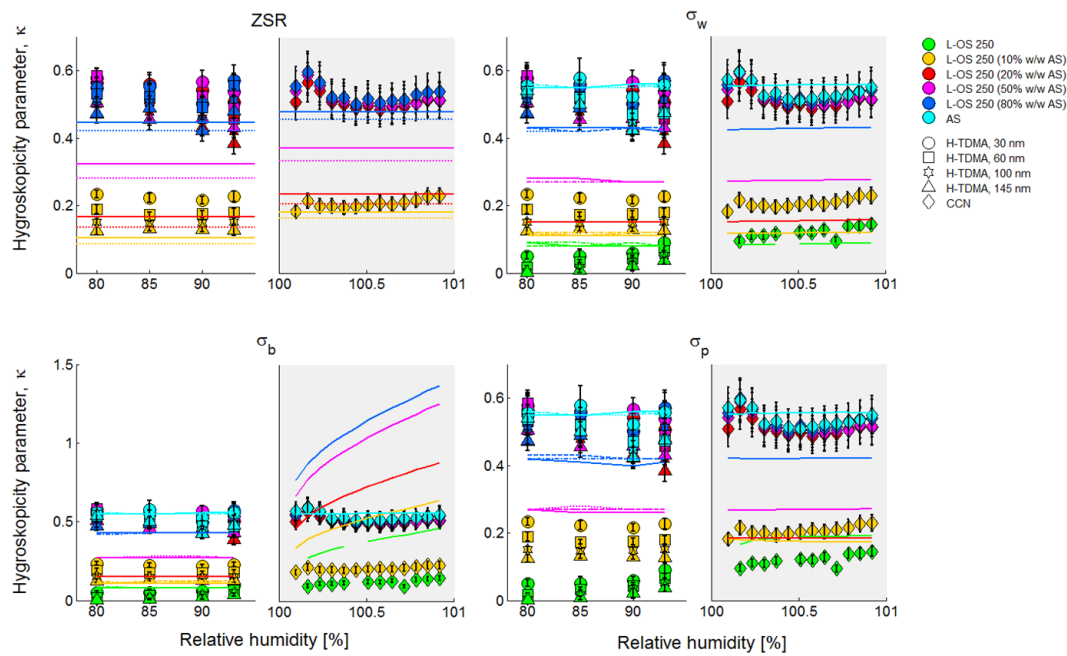


**Figure 9.** Measured and modelled hygroscopicity parameter,  $\kappa$ , as a function of RH for six mixtures of L-OS 250 and AS. Markers represent the measured values of  $\kappa$  and lines represent the modelled values of  $\kappa$ . The light grey area denotes humidity in the supersaturated range (CCN) and the white area denotes humidity in the subsaturated range (H-TDMA). For subfigure ZSR the solid lines represent additive  $\kappa$  calculated using a density of  $1.176 \text{ g cm}^{-3}$  for L-OS 250 whereas a density of  $1.7 \text{ g cm}^{-3}$  is represented with the dotted lines. For subfigure  $\sigma_w$ ,  $\sigma_b$  and  $\sigma_p$  the subsaturated range, the solid line is modelled  $\kappa$  for 30 nm particles, the dash-dotted line is modelled  $\kappa$  for 60 nm particles, the dotted line is modelled  $\kappa$  for 100 nm particles and the dashed line is modelled  $\kappa$  for 145 nm particles. Error bars represent the uncertainty on the  $\kappa$  values obtained from the measurements ( $\pm 10\%$  on  $\kappa_{\text{CCN}}$  and  $\pm 2$  standard deviation on  $\kappa_{\text{H-TDMA}}$ ). Please note that the y axis in subfigure  $\sigma_b$  is different from the other subfigures.

in the Köhler models, rather than being a direct consequence of L-OS 250 surface activity.

One striking feature is that the bulk surfactant model  $\sigma_b$  is clearly not able to predict measured aerosol water uptake and droplet activation in the supersaturated humidity range, where  $\sigma_b$  predicts a significant increase in  $\kappa$  with supersaturation for all particles comprising L-OS 250. This has been found consistently in previous studies of both pure surfactant and mixed surfactant/salt systems (Prisle et al., 2008, 2010b, 2011). The  $\sigma_w$  model is much better at reproducing experimental data, but again the model is not able to predict the non-linear composition dependency, since also this model is purely a bulk solution representation. Finally, the  $\sigma_p$  model is able to predict the magnitude of the pure L-OS 250  $\kappa_{\text{CCN}}$  value and also the increasing trend with increasing  $\text{SS}_c$ , but again the model is not able to predict the non-linear composition dependency. This strongly suggests that partitioning effects do in fact influence activation thermodynamics of L-OS 250, even if the overall  $\kappa$  values may be subject to cancellation effects between surface tension decrease and surface partitioning, as was found for other atmospheric surfactants (Prisle et al., 2008, 2010b); however, partitioning does not seem to drive the variation in water uptake between the sub- or supersaturated regimes. Thus, droplet non-ideality

( $\gamma_w = 1$ ) may also play a role for the observed non-linear  $\kappa$  variations with particle composition. These findings are in good agreement with those from Prisle et al. (2010b), who showed that bulk solution surface tensions should not be used for microscopic droplets without also accounting for bulk-to-surface partitioning.

#### 4 Cloud-forming potential of organosulfates and model implications

Atmospheric aerosols are very complex, often consisting of many thousand organic compounds (Hamilton et al., 2004; Hallquist et al., 2009), and thus the two-component particles studied here are probably not fully representative for atmospheric aerosols. However investigation of simplified systems can reveal the important interactions between complex organic compounds and common inorganics, which may influence cloud activation as well as expose how  $\kappa$  is influenced by the mixing ratio of organics to inorganics. Based on the results presented in the previous sections, we here try to evaluate the cloud-forming potential of organosulfates and the possible implications of our results for climate models.

From our measurements, it was clear that L-OS 250 is indeed surface active and decreases the surface tension of water considerably, even for mixtures where the L-OS 250 concentrations were as low as 5 % of total solute concentration. However, the low intrinsic  $\kappa$  values for L-OS 250 showed the organosulfate to be modestly hygroscopic; hence in terms of water uptake, the significant surface tension effect must be countered by other effects in the droplets, such as simultaneous bulk-to-surface partitioning or limited water solubility. Based on the results presented here, the intrinsic cloud-forming properties of pure L-OS 250 thus appear to be limited. On its own, L-OS 250 particles require significantly higher SS to activate into cloud droplets compared to inorganic salts such as AS. However, L-OS 250 does not appear to inhibit the CCN activity of very CCN active inorganics such as AS beyond displacing the AS mass in the aerosol, since the hygroscopic properties of mixtures of L-OS 250 and AS converged towards the properties of pure AS when AS composed  $\geq 20\%$  w/w of the mixture. In fact, when particles with as much as 80 % by mass of L-OS 250 display the same water uptake properties as pure AS particles of the same dry diameter, it shows a significant contribution of the organic and/or its interactions with the inorganic. The discrepancy between  $\kappa_{\text{H-TDMA}}$  and  $\kappa_{\text{CCN}}$  for L-OS 250 shows that extrapolation of  $\kappa$  from the subsaturated to the supersaturated range is connected with significant uncertainties. In regard to the cloud-forming potential of L-OS 250 it should therefore be emphasised that the CCNC measurements are of greater importance as clouds are supersaturated with water.

The results presented in Sect. 3.4.4 are important for global climate models, as the surface activity representations,  $\sigma_w$ ,  $\sigma_b$  and  $\sigma_p$ , tested here may be used in such models. From Fig. 9 it is clear that  $\sigma_b$  in particular fails to represent the experimental data at supersaturated conditions. When a representation corresponding to the  $\sigma_b$  model is implemented in global simulations of droplet activation, the predicted cloud droplet number is much larger than when  $\sigma_w$  or  $\sigma_p$  is used (Prisle et al., 2012); hence  $\sigma_b$  predicts a greater indirect aerosol effect than the two other models. Our results imply that  $\sigma_b$  should not be used in global simulations to represent cloud droplet activation of (surface active) organics as it cannot reproduce experimental data on the process level. Introducing  $\sigma_b$  in climate models would thus result in even larger uncertainties on the predictions of the future climate.

Concerning global climate models it is of high interest to consider whether organosulfates can be merged with other organics and represented by one common  $\kappa$  value. The  $\kappa$  values found here are within the range of other organics (approximately 0.0 to 0.3 for CCNC measurements), including carboxylic acids, sugars and HULIS (Petters and Kreidenweis, 2007; Chan et al., 2008; Jing et al., 2015). Hence, considering  $\kappa$  alone, it would seem that organosulfates can be merged with other organics; however, this study reveals how organosulfates behave on their own and in mixtures with inorganics, but this is not necessarily representative for com-

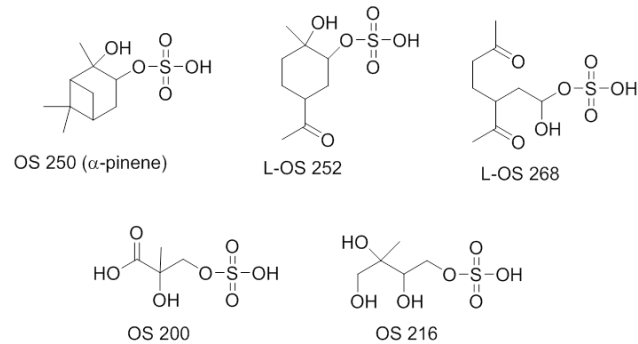


**Figure 10.** Selected organosulfates derived from monoterpenes and isoprene (Surratt et al., 2007, 2008). Note that isomers are possible for the given structures.

plex organic mixtures. For example a recent study by Jing et al. (2015) shows that  $\kappa$  of organic mixtures can be much higher compared to what was expected by considering  $\kappa$  of the individual compounds; hence we do not think that all organics can be represented in climate models by one common  $\kappa$  value based on the mean of individual  $\kappa$  values (essentially the ZSR representation).

L-OS 250 is but one of many organosulfates found in the atmosphere, but we believe that the hygroscopic properties found for L-OS 250 in this study is a good representation for (at least some of the) other monoterpene-derived organosulfates, for example OS 250 derived from  $\alpha$ -/ $\beta$ -pinene, L-OS 252 and L-OS 268, since they have structural similarities and few functional groups (see Fig. 10). Many organosulfates of atmospheric relevance contain additional hydroxyl groups or carboxylic acid groups and are composed of fewer carbon atoms than L-OS 250, for example OS 200 and OS 216 derived from isoprene (see Fig. 10). These organosulfates with additional hydroxyl/carboxylic acid groups are likely to be more hygroscopic and therefore more prone to activate into cloud droplets, according to the recent study by Suda et al. (2014) showing that hygroscopicity of organics increases with addition of hydroxyl groups, carboxylic acid groups and hydroperoxide groups, in the given order. There is thus a need for further hygroscopicity measurements to investigate the atmospheric impact and cloud-forming potential of smaller and more polar organosulfates, e.g. those derived from isoprene.

## 5 Conclusions

We have here presented the first characterisation of an atmospherically relevant organosulfate, derived from limonene (L-OS 250), in terms of surface activity and hygroscopic properties. Surface tension measurements showed L-OS 250 to be surface active with the capacity to decrease the surface tension of bulk aqueous solutions considerably. The surface tension of L-OS 250 solutions decreased even further with

the addition of AS, suggesting a salting out effect in bulk solutions. The significant surface activity of L-OS 250 suggests that L-OS 250 could act as a CCN.

The hygroscopic properties of particles containing L-OS 250, AS and mixtures hereof were examined at sub- and supersaturated conditions using a custom-built set-up, allowing parallel measurements of HGF (with an H-TDMA) and of CCN activation (with a CCNC). HGF for L-OS 250 was found to increase from 1.0 (no growth) to 1.2 over the measured humidity range from 80 to 93 %, showing that L-OS 250 can take up water in the subsaturated range. However, compared to AS (HGF = 1.4 at 80 % RH and 1.9 at 93 % RH) the investigated L-OS 250 particles only showed weak hygroscopic growth. Measurement with the CCNC showed the ability of L-OS 250 to activate into cloud droplets; the critical particle diameters for L-OS 250 particles were 55–83 % larger than for pure AS, which is comparable to critical particle diameters for other atmospheric organics previously characterized. The hygroscopic properties of the L-OS 250/AS system showed a non-linear composition dependency, as both HGF values and d<sub>50</sub> of the mixed particles with  $\geq 20\% \text{ w/w AS}$  converged toward the values of pure AS. This implies that L-OS 250 actually contribute to the overall hygroscopicity of these mixed particles. The hygroscopicity parameter,  $\kappa$ , was calculated for the L-OS 250/AS system, revealing L-OS 250 to be weakly hygroscopic.  $\kappa$  derived from the H-TDMA measurements was found to vary with particle diameter for all particle compositions, increasing with decreasing particle dry diameter. However, whether  $\kappa_{\text{H-TDMA}}$  is truly size dependent or an experimental artefact has caused this trend cannot be concluded from these experiments alone.  $\kappa_{\text{CCN}}$  was larger than  $\kappa_{\text{H-TDMA}}$  for L-OS 250, which is probably caused by differences in the degree of dissolution of L-OS 250 at sub- and supersaturated conditions. For AS and mixed L-OS 250/AS particles  $\kappa_{\text{CCN}}$  and  $\kappa_{\text{H-TDMA}}$  were in the same range, but with significant variation. Both HGF and d<sub>50</sub> displayed non-linear composition dependency, as reflected in sub- and supersaturated  $\kappa$  values.

It was investigated whether the hygroscopic properties of the L-OS 250/AS system could be reproduced by model calculations under different assumptions concerning surface tension effects and bulk-to-surface partitioning. Based on the model calculations,  $\kappa$  was calculated and compared with the experimental  $\kappa$  values. None of the three model calculations or the ZSR mixing rule were able to capture the observed non-linear composition dependency for the mixed particles, indicating that L-OS 250 solubility and non-ideal droplet interactions could be important for mixtures of the L-OS 250/AS system, as these were not accounted for by any of the models. The bulk solution representation of model  $\sigma_b$  was especially erroneous in reproducing the experimental  $\kappa$  values of the system, underlining that  $\sigma_b$  should not be used in global climate models to represent cloud activation properties of surface active organics.

**The Supplement related to this article is available online at doi:10.5194/acp-15-14071-2015-supplement.**

**Acknowledgements.** This research was financially supported by NordForsk (Nordic Council of Ministers) through the Nordic Centre of Excellence Cryosphere-Atmosphere Interactions in a Changing Arctic Climate (CRAICC) and the VILLUM Foundation. The research leading to these results has received funding from the European Union Seventh Framework Programme (FP7/2007-2013) under grant agreement no. 262254 and via H2020 under ACTRIS2. The work was partly supported by the Office of Science (BER), US Department of Energy via Biogenic Aerosols – Effects on Clouds and Climate (BAECC). N. L. Prisle gratefully acknowledges the personal funding received for this work from the Finnish Academy of Sciences (grant 257411) and A. Virtanen thankfully acknowledges funding received from ERC (grant QAPPA 335478) and Academy Grant (259005). The authors would also like to thank Ulla Wideqvist, Johan Ström and Hans Christen Hansson for use of the tensiometer at ITM, Stockholm University, and Mikhail Paramonov for providing Matlab scripts for calculation of  $\kappa_{\text{CCN}}$  and help regarding calibration of the CCNC instrument.

Edited by: D. Topping

## References

- Asa-Awuku, A., Engelhart, G. J., Lee, B. H., Pandis, S. N., and Nenes, A.: Relating CCN activity, volatility, and droplet growth kinetics of  $\beta$ -caryophyllene secondary organic aerosol, *Atmos. Chem. Phys.*, 9, 795–812, doi:10.5194/acp-9-795-2009, 2009.
- Carrico, C. M., Petters, M. D., Kreidenweis, S. M., Collett, J. L., Engling, G., and Malm, W. C.: Aerosol hygroscopicity and cloud droplet activation of extracts of filters from biomass burning experiments, *J. Geophys. Res.-Atmos.*, 113, D08206, doi:10.1029/2007jd009274, 2008.
- Cavdar, H. and Saracoğlu, N.: Ring opening of epoxides with  $\text{NaHSO}_4$ : isolation of beta-hydroxy sulfate esters and an effective synthesis for trans-diols, *Tetrahedron*, 65, 985–989, doi:10.1016/j.tet.2008.11.092, 2009.
- Cerully, K. M., Raatikainen, T., Lance, S., Tkacik, D., Tiitta, P., Petäjä, T., Ehn, M., Kulmala, M., Worsnop, D. R., Laaksonen, A., Smith, J. N., and Nenes, A.: Aerosol hygroscopicity and CCN activation kinetics in a boreal forest environment during the 2007 EUCAARI campaign, *Atmos. Chem. Phys.*, 11, 12369–12386, doi:10.5194/acp-11-12369-2011, 2011
- Chan, M. N., Kreidenweis, S. M., and Chan, C. K.: Measurements of the hygroscopic and deliquescence properties of organic compounds of different solubilities in water and their relationship with cloud condensation nuclei activities, *Environ. Sci. Technol.*, 42, 3602–3608, doi:10.1021/es7023252, 2008.
- Cheng, Y., Li, S. M., Leithead, A., Brickell, P. C., and Leaitch, W. R.: Characterizations of cis-pinonic acid and n-fatty acids on fine aerosols in the Lower Fraser Valley during Pacific 2001 Air Quality Study, *Atmos. Environ.*, 38, 5789–5800, doi:10.1016/j.atmosenv.2004.01.051, 2004.

- Clegg, S. L., Brimblecombe, P., and Wexler, A. S.: Thermodynamic model of the system  $\text{H}^+ \text{-NH}_4^+ \text{-Na}^+ \text{-SO}_4^{2-} \text{-NO}_3^- \text{-Cl}^- \text{-H}_2\text{O}$  at 298.15 K, *J. Phys. Chem. A*, 102, 2155–2171, doi:10.1021/Jp973043j, 1998.
- Cruz, C. N. and Pandis, S. N.: Deliquescence and hygroscopic growth of mixed inorganic-organic atmospheric aerosol, *Environ. Sci. Technol.*, 34, 4313–4319, doi:10.1021/Es9907109, 2000.
- Dusek, U., Frank, G. P., Massling, A., Zeromskiene, K., Iinuma, Y., Schmid, O., Helas, G., Hennig, T., Wiedensohler, A., and Andreae, M. O.: Water uptake by biomass burning aerosol at sub- and supersaturated conditions: closure studies and implications for the role of organics, *Atmos. Chem. Phys.*, 11, 9519–9532, doi:10.5194/acp-11-9519-2011, 2011.
- Ekström, S., Nozière, B., and Hansson, H.-C.: The Cloud Condensation Nuclei (CCN) properties of 2-methyltetrols and C3–C6 polyols from osmolality and surface tension measurements, *Atmos. Chem. Phys.*, 9, 973–980, doi:10.5194/acp-9-973-2009, 2009.
- Facchini, M. C., Mircea, M., Fuzzi, S., and Charlson, R. J.: Cloud albedo enhancement by surface-active organic solutes in growing droplets, *Nature*, 401, 257–259, doi:10.1038/45758, 1999.
- Frossard, A. A., Shaw, P. M., Russell, L. M., Kroll, J. H., Canagaratna, M. R., Worsnop, D. R., Quinn, P. K., and Bates, T. S.: Springtime Arctic haze contributions of submicron organic particles from European and Asian combustion sources, *J. Geophys. Res.-Atmos.*, 116, D05205, doi:10.1029/2010jd015178, 2011.
- Froyd, K. D., Murphy, S. M., Murphy, D. M., de Gouw, J. A., Eddingsaas, N. C., and Wennberg, P. O.: Contribution of isoprene-derived organosulfates to free tropospheric aerosol mass, *P. Natl. Acad. Sci. USA*, 107, 21360–21365, doi:10.1073/pnas.1012561107, 2010.
- Good, N., Topping, D. O., Allan, J. D., Flynn, M., Fuentes, E., Irwin, M., Williams, P. I., Coe, H., and McFiggans, G.: Consistency between parameterisations of aerosol hygroscopicity and CCN activity during the RHAMBLe discovery cruise, *Atmos. Chem. Phys.*, 10, 3189–3203, doi:10.5194/acp-10-3189-2010, 2010.
- Gysel, M., Crosier, J., Topping, D. O., Whitehead, J. D., Bower, K. N., Cubison, M. J., Williams, P. I., Flynn, M. J., McFiggans, G. B., and Coe, H.: Closure study between chemical composition and hygroscopic growth of aerosol particles during TORCH2, *Atmos. Chem. Phys.*, 7, 6131–6144, doi:10.5194/acp-7-6131-2007, 2007.
- Gysel, M., McFiggans, G. B., and Coe, H.: Inversion of tandem differential mobility analyser (TDMA) measurements, *J. Aerosol. Sci.*, 40, 134–151, doi:10.1016/j.jaerosci.2008.07.013, 2009.
- Hallquist, M., Wenger, J. C., Baltensperger, U., Rudich, Y., Simpson, D., Claeys, M., Dommen, J., Donahue, N. M., George, C., Goldstein, A. H., Hamilton, J. F., Herrmann, H., Hoffmann, T., Iinuma, Y., Jang, M., Jenkin, M. E., Jimenez, J. L., Kiendler-Scharr, A., Maenhaut, W., McFiggans, G., Mentel, Th. F., Monod, A., Prévôt, A. S. H., Seinfeld, J. H., Surratt, J. D., Szmigielski, R., and Wildt, J.: The formation, properties and impact of secondary organic aerosol: current and emerging issues, *Atmos. Chem. Phys.*, 9, 5155–5236, doi:10.5194/acp-9-5155-2009, 2009.
- Hämeri, K., Charlson, R., and Hansson, H. C.: Hygroscopic properties of mixed ammonium sulfate and carboxylic acids particles, *Aiche J.*, 48, 1309–1316, doi:10.1002/aic.690480617, 2002.
- Hamilton, J. F., Webb, P. J., Lewis, A. C., Hopkins, J. R., Smith, S., and Davy, P.: Partially oxidised organic components in urban aerosol using GCXGC-TOF/MS, *Atmos. Chem. Phys.*, 4, 1279–1290, doi:10.5194/acp-4-1279-2004, 2004.
- Hansen, A. M. K., Kristensen, K., Nguyen, Q. T., Zare, A., Cozzi, F., Nøjgaard, J. K., Skov, H., Brandt, J., Christensen, J. H., Ström, J., Tunved, P., Krejci, R., and Glasius, M.: Organosulfates and organic acids in Arctic aerosols: speciation, annual variation and concentration levels, *Atmos. Chem. Phys.*, 14, 7807–7823, doi:10.5194/acp-14-7807-2014, 2014.
- Henning, S., Ziese, M., Kiselev, A., Saathoff, H., Möhler, O., Mentel, T. F., Buchholz, A., Spindler, C., Michaud, V., Monier, M., Sellegri, K., and Stratmann, F.: Hygroscopic growth and droplet activation of soot particles: uncoated, succinic or sulfuric acid coated, *Atmos. Chem. Phys.*, 12, 4525–4537, doi:10.5194/acp-12-4525-2012, 2012.
- Hersey, S. P., Craven, J. S., Metcalf, A. R., Lin, J., Lathem, T., Suski, K. J., Cahill, J. F., Duong, H. T., Sorooshian, A., Jonsson, H. H., Shiraiwa, M., Zuend, A., Nenes, A., Prather, K. A., Flagan, R. C., and Seinfeld, J. H.: Composition and hygroscopicity of the Los Angeles Aerosol: CalNex, *J. Geophys. Res.-Atmos.*, 118, 3016–3036, doi:10.1002/Jgrd.50307, 2013.
- Holmgren, H., Sellegri, K., Hervo, M., Rose, C., Freney, E., Viliani, P., and Laj, P.: Hygroscopic properties and mixing state of aerosol measured at the high-altitude site Puy de Dôme (1465 m a.s.l.), France, *Atmos. Chem. Phys.*, 14, 9537–9554, doi:10.5194/acp-14-9537-2014, 2014.
- Hong, J., Häkkinen, S. A. K., Paramonov, M., Äijälä, M., Hakala, J., Nieminen, T., Mikkilä, J., Prisle, N. L., Kulmala, M., Riipinen, I., Bilde, M., Kerminen, V.-M., and Petäjä, T.: Hygroscopicity, CCN and volatility properties of submicron atmospheric aerosol in a boreal forest environment during the summer of 2010, *Atmos. Chem. Phys.*, 14, 4733–4748, doi:10.5194/acp-14-4733-2014, 2014.
- Iinuma, Y., Muller, C., Berndt, T., Boge, O., Claeys, M., and Herrmann, H.: Evidence for the existence of organosulfates from beta-pinene ozonolysis in ambient secondary organic aerosol, *Environ. Sci. Technol.*, 41, 6678–6683, doi:10.1021/es070938t, 2007.
- IPCC: Summary for Policymakers, Cambridge University Press, Cambridge, United Kingdom and New York, NY, USA, 2013.
- Jing, B., Tong, S. R., Liu, Q. F., Li, K., Wang, W. G., Zhang, Y. H., and Ge, M. F.: Hygroscopic behavior of multicomponent organic aerosols and their internal mixtures with ammonium sulfate, *Atmos. Chem. Phys. Discuss.*, 15, 23357–23405, doi:10.5194/acpd-15-23357-2015, 2015.
- Kiss, G., Tombacz, E., and Hansson, H. C.: Surface tension effects of humic-like substances in the aqueous extract of tropospheric fine aerosol, *J. Atmos. Chem.*, 50, 279–294, doi:10.1007/s10874-005-5079-5, 2005.
- Koehler, K. A., Kreidenweis, S. M., DeMott, P. J., Prenni, A. J., Carrico, C. M., Ervens, B., and Feingold, G.: Water activity and activation diameters from hygroscopicity data – Part II: Application to organic species, *Atmos. Chem. Phys.*, 6, 795–809, doi:10.5194/acp-6-795-2006, 2006.

- Kreidenweis, S. M., Petters, M. D., and DeMott, P. J.: Deliquescence-controlled activation of organic aerosols, *Geophys. Res. Lett.*, 33, L06801, doi:10.1029/2005gl024863, 2006.
- Kristensen, K. and Glasius, M.: Organosulfates and oxidation products from biogenic hydrocarbons in fine aerosols from a forest in North West Europe during spring, *Atmos. Environ.*, 45, 4546–4556, doi:10.1016/j.atmosenv.2011.05.063, 2011.
- Kristensen, T. B., Prisle, N. L., and Bilde, M.: Cloud droplet activation of mixed model HULIS and NaCl particles: Experimental results and kappa-Kohler theory, *Atmos. Res.*, 137, 167–175, doi:10.1016/j.atmosres.2013.09.017, 2014.
- Lee, J. Y. and Hildemann, L. M.: Surface tension of solutions containing dicarboxylic acids with ammonium sulfate, D-glucose, or humic acid, *J. Aerosol. Sci.*, 64, 94–102, doi:10.1016/j.jaerosci.2013.06.004, 2013.
- Lin, P., Huang, X. F., He, L. Y., and Yu, J. Z.: Abundance and size distribution of HULIS in ambient aerosols at a rural site in South China, *J. Aerosol. Sci.*, 41, 74–87, doi:10.1016/j.jaerosci.2009.09.001, 2010.
- Lin, Y. H., Zhang, Z. F., Docherty, K. S., Zhang, H. F., Budisulistiorini, S. H., Rubitschun, C. L., Shaw, S. L., Knipping, E. M., Edgerton, E. S., Kleindienst, T. E., Gold, A., and Suratt, J. D.: Isoprene Epoxydiols as Precursors to Secondary Organic Aerosol Formation: Acid-Catalyzed Reactive Uptake Studies with Authentic Compounds, *Environ. Sci. Technol.*, 46, 250–258, doi:10.1021/es202554c, 2012.
- Massling, A., Stock, M., Wehner, B., Wu, Z. J., Hu, M., Bruggemann, E., Gnauk, T., Herrmann, H., and Wiedensohler, A.: Size segregated water uptake of the urban submicrometer aerosol in Beijing, *Atmos. Environ.*, 43, 1578–1589, doi:10.1016/j.atmosenv.2008.06.003, 2009.
- Massoli, P., Lambe, A. T., Ahern, A. T., Williams, L. R., Ehn, M., Mikkilä, J., Canagaratna, M. R., Brune, W. H., Onasch, T. B., Jayne, J. T., Petäjä, T., Kulmala, M., Laaksonen, A., Kolb, C. E., Davidovits, P., and Worsnop, D. R.: Relationship between aerosol oxidation level and hygroscopic properties of laboratory generated secondary organic aerosol (SOA) particles, *Geophys. Res. Lett.*, 37, L24801, doi:10.1029/2010gl045258, 2010.
- Matubayasi, N.: Surface Tension and Related Thermodynamic Quantities of Aqueous Electrolyte Solutions, CRC Press, Boca Raton, Florida, 2013.
- Mochida, M., Kitamori, Y., Kawamura, K., Nojiri, Y., and Suzuki, K.: Fatty acids in the marine atmosphere: Factors governing their concentrations and evaluation of organic films on sea-salt particles, *J. Geophys. Res.-Atmos.*, 107, 4325, doi:10.1029/2001jd001278, 2002.
- Nguyen, Q. T., Christensen, M. K., Cozzi, F., Zare, A., Hansen, A. M. K., Kristensen, K., Tulinius, T. E., Madsen, H. H., Christensen, J. H., Brandt, J., Massling, A., Nøjgaard, J. K., and Glasius, M.: Understanding the anthropogenic influence on formation of biogenic secondary organic aerosols in Denmark via analysis of organosulfates and related oxidation products, *Atmos. Chem. Phys.*, 14, 8961–8981, doi:10.5194/acp-14-8961-2014, 2014.
- Noziere, B., Baduel, C., and Jaffrezo, J. L.: The dynamic surface tension of atmospheric aerosol surfactants reveals new aspects of cloud activation, *Nat. Commun.*, 5, 3335, doi:10.1038/Ncomms4335, 2014.
- Pajunoja, A., Lambe, A. T., Hakala, J., Rastak, N., Cummings, M. J., Brogan, J. F., Hao, L., Paramonov, M., Hong, J., Prisle, N. L., Malila, J., Romakkaniemi, S., Lehtinen, K. E. J., Laaksonen, A., Kulmala, M., Massoli, P., Onasch, T. B., Donahue, N. M., Riipinen, I., Davidovits, P., Worsnop, D. R., Petäjä, T., and Virtanen, A.: Adsorptive uptake of water by semisolid secondary organic aerosols, *Geophys. Res. Lett.*, 42, 3063–3068, doi:10.1002/2015gl063142, 2015.
- Paramonov, M., Aalto, P. P., Asmi, A., Prisle, N., Kerminen, V.-M., Kulmala, M., and Petäjä, T.: The analysis of size-segregated cloud condensation nuclei counter (CCNC) data and its implications for cloud droplet activation, *Atmos. Chem. Phys.*, 13, 10285–10301, doi:10.5194/acp-13-10285-2013, 2013.
- Petters, M. D. and Kreidenweis, S. M.: A single parameter representation of hygroscopic growth and cloud condensation nucleus activity, *Atmos. Chem. Phys.*, 7, 1961–1971, doi:10.5194/acp-7-1961-2007, 2007.
- Petters, M. D., Wex, H., Carrico, C. M., Hallbauer, E., Massling, A., McMeeking, G. R., Poulain, L., Wu, Z., Kreidenweis, S. M., and Stratmann, F.: Towards closing the gap between hygroscopic growth and activation for secondary organic aerosol – Part 2: Theoretical approaches, *Atmos. Chem. Phys.*, 9, 3999–4009, doi:10.5194/acp-9-3999-2009, 2009.
- Prenni, A. J., Petters, M. D., Kreidenweis, S. M., DeMott, P. J., and Ziemann, P. J.: Cloud droplet activation of secondary organic aerosol, *J. Geophys. Res.-Atmos.*, 112, D10223, doi:10.1029/2006jd007963, 2007.
- Prisle, N. L.: Cloud Condensation Nuclei Properties of Organic Aerosol Particles: Effects of Acid Dissociation and Surfactant Partitioning, MSc Thesis, Department of Chemistry, Faculty of Science, University of Copenhagen, Copenhagen, Denmark, 2006.
- Prisle, N. L., Raatikainen, T., Sorjamaa, R., Svenssonsson, B., Laaksonen, A., and Bilde, M.: Surfactant partitioning in cloud droplet activation: a study of C8, C10, C12 and C14 normal fatty acid sodium salts, *Tellus B, C* 60, 416–431, doi:10.1111/j.1600-0889.2008.00352.x, 2008.
- Prisle, N. L., Engelhart, G. J., Bilde, M., and Donahue, N. M.: Humidity influence on gas-particle phase partitioning of alpha-pinene + O<sub>3</sub> secondary organic aerosol, *Geophys. Res. Lett.*, 37, L01802, doi:10.1029/2009gl041402, 2010a.
- Prisle, N. L., Raatikainen, T., Laaksonen, A., and Bilde, M.: Surfactants in cloud droplet activation: mixed organic-inorganic particles, *Atmos. Chem. Phys.*, 10, 5663–5683, doi:10.5194/acp-10-5663-2010, 2010b.
- Prisle, N. L., Dal Maso, M., and Kokkola, H.: A simple representation of surface active organic aerosol in cloud droplet formation, *Atmos. Chem. Phys.*, 11, 4073–4083, doi:10.5194/acp-11-4073-2011, 2011.
- Prisle, N. L., Asmi, A., Topping, D., Partanen, A. I., Romakkaniemi, S., Dal Maso, M., Kulmala, M., Laaksonen, A., Lehtinen, K. E. J., McFiggans, G., and Kokkola, H.: Surfactant effects in global simulations of cloud droplet activation, *Geophys. Res. Lett.*, 39, L05802, doi:10.1029/2011gl050467, 2012.
- Rose, D., Gunthe, S. S., Mikhailov, E., Frank, G. P., Dusek, U., Andreae, M. O., and Pöschl, U.: Calibration and measurement uncertainties of a continuous-flow cloud condensation nuclei counter (DMT-CCNC): CCN activation of ammonium sulfate and sodium chloride aerosol particles in theory and experiment,

- Atmos. Chem. Phys., 8, 1153–1179, doi:10.5194/acp-8-1153-2008, 2008.
- Rose, D., Nowak, A., Achtert, P., Wiedensohler, A., Hu, M., Shao, M., Zhang, Y., Andreae, M. O., and Pöschl, U.: Cloud condensation nuclei in polluted air and biomass burning smoke near the mega-city Guangzhou, China – Part 1: Size-resolved measurements and implications for the modeling of aerosol particle hygroscopicity and CCN activity, *Atmos. Chem. Phys.*, 10, 3365–3383, doi:10.5194/acp-10-3365-2010, 2010.
- Seinfeld, J. H. and Pandis, S. N.: *Atmospheric Chemistry and Physics: From Air Pollution to Climate Change*, 2nd Edn., Wiley, Hoboken, New Jersey, 2006.
- Sjogren, S., Gysel, M., Weingartner, E., Alfarra, M. R., Duplissy, J., Cozic, J., Crosier, J., Coe, H., and Baltensperger, U.: Hygroscopicity of the submicrometer aerosol at the high-alpine site Jungfraujoch, 3580 m a.s.l., Switzerland, *Atmos. Chem. Phys.*, 8, 5715–5729, doi:10.5194/acp-8-5715-2008, 2008.
- Song, J. Z., He, L. L., Peng, P. A., Zhao, J. P., and Ma, S. X.: Chemical and Isotopic Composition of Humic-Like Substances (HULIS) in Ambient Aerosols in Guangzhou, South China, *Aerosol. Sci. Tech.*, 46, 533–546, doi:10.1080/02786826.2011.645956, 2012.
- Sorjamaa, R., Svenningsson, B., Raatikainen, T., Henning, S., Bilde, M., and Laaksonen, A.: The role of surfactants in Köhler theory reconsidered, *Atmos. Chem. Phys.*, 4, 2107–2117, doi:10.5194/acp-4-2107-2004, 2004.
- Stokes, R. H. and Robinson, R. A.: Interactions in Aqueous Nonelectrolyte Solutions I. Solute-Solvent Equilibria, *J. Phys. Chem.-US*, 70, 2126–2131, doi:10.1021/J100879a010, 1966.
- Suda, S. R., Petters, M. D., Yeh, G. K., Strollo, C., Matsunaga, A., Faulhaber, A., Ziemann, P. J., Prenni, A. J., Carrico, C. M., Sullivan, R. C., and Kreidenweis, S. M.: Influence of Functional Groups on Organic Aerosol Cloud Condensation Nucleus Activity, *Environ. Sci. Technol.*, 48, 10182–10190, doi:10.1021/Es502147y, 2014.
- Surratt, J. D., Kroll, J. H., Kleindienst, T. E., Edney, E. O., Claeys, M., Soroshian, A., Ng, N. L., Offenberg, J. H., Lewandowski, M., Jaoui, M., Flagan, R. C., and Seinfeld, J. H.: Evidence for organosulfates in secondary organic aerosol, *Environ. Sci. Technol.*, 41, 517–527, doi:10.1021/Es062081q, 2007.
- Surratt, J. D., Gómez-González, Y., Chan, A. W. H., Vermeylen, R., Shahgholi, M., Kleindienst, T. E., Edney, E. O., Offenberg, J. H., Lewandowski, M., Jaoui, M., Maenhaut, W., Claeys, M., Flagan, R. C., and Seinfeld, J. H.: Organosulfate formation in biogenic secondary organic aerosol, *J. Phys. Chem. A*, 112, 8345–8378, doi:10.1021/Jp802310p, 2008.
- Swietlicki, E., Hansson, H. C., Hämeri, K., Svenningsson, B., Massling, A., McFiggans, G., McMurry, P. H., Petäjä, T., Tunved, P., Gysel, M., Topping, D., Weingartner, E., Baltensperger, U., Rissler, J., Wiedensohler, A., and Kulmala, M.: Hygroscopic properties of submicrometer atmospheric aerosol particles measured with H-TDMA instruments in various environments – a review, *Tellus B*, 60, 432–469, doi:10.1111/j.1600-0889.2008.00350.x, 2008.
- Topping, D.: An analytical solution to calculate bulk mole fractions for any number of components in aerosol droplets after considering partitioning to a surface layer, *Geosci. Model Dev.*, 3, 635–642, doi:10.5194/gmd-3-635-2010, 2010.
- Wex, H., McFiggans, G., Henning, S., and Stratmann, F.: Influence of the external mixing state of atmospheric aerosol on derived CCN number concentrations, *Geophys. Res. Lett.*, 37, L10805, doi:10.1029/2010gl043337, 2010.
- Wu, Z. J., Poulain, L., Henning, S., Dieckmann, K., Birmili, W., Merkel, M., van Pinxteren, D., Spindler, G., Müller, K., Stratmann, F., Herrmann, H., and Wiedensohler, A.: Relating particle hygroscopicity and CCN activity to chemical composition during the HCCT-2010 field campaign, *Atmos. Chem. Phys.*, 13, 7983–7996, doi:10.5194/acp-13-7983-2013, 2013.
- Zardini, A. A., Sjogren, S., Marcolli, C., Krieger, U. K., Gysel, M., Weingartner, E., Baltensperger, U., and Peter, T.: A combined particle trap/HTDMA hygroscopicity study of mixed inorganic/organic aerosol particles, *Atmos. Chem. Phys.*, 8, 5589–5601, doi:10.5194/acp-8-5589-2008, 2008.